Impact of Solar Geoengineering on Wildfires in the 21st Century in CESM2/WACCM6

Wenfu Tang[1], Simone Tilmes[1], David M. Lawrence[2], Fang Li[3], Cenlin He[4], Louisa K. Emmons[1], Rebecca R. Buchholz[1], Lili Xia[5]

[1]Atmospheric Chemistry Observations & Modeling Laboratory, National Center for Atmospheric Research, Boulder, CO, USA
[2]Climate and Global Dynamics Laboratory, National Center for Atmospheric Research, Boulder, CO, USA
[3]International Center for Climate and Environment Sciences, Institute of Atmospheric Physics, Chinese Academy of Sciences, Beijing, China
[4]Research Applications Laboratory, National Center for Atmospheric Research, Boulder, CO, USA
[5]Department of Environmental Sciences, Rutgers University, New Brunswick, NJ, USA

Correspondence: Wenfu Tang (wenfut@ucar.edu)

Abstract

We quantify future changes of wildfire burned area and carbon emissions in the 21st century under four Shared Socioeconomic Pathways (SSPs) scenarios and two SSP5-8.5-based solar geoengineering scenarios with a target surface temperature defined by SSP2-4.5: solar irradiance reduction (G6solar) and stratospheric sulfate aerosol injections (G6sulfur), and explore the mechanisms that drive solar geoengineering impacts on fires. This study is based on fully coupled climate-chemistry simulations with simulated occurrence of fires (area burnt and carbon emissions) using the Whole Atmosphere Community Climate Model Version 6 (WACCM6) as the atmospheric component of the Community Earth System Model Version 2 (CESM2). Globally, total wildfire burned area is projected to increase over the 21st century under scenarios without geoengineering and decrease under the two geoengineering scenarios. By the end of the century, the two geoengineering scenarios have lower burned area and fire carbon emissions than not only their base-climate scenario SSP5-8.5 but also the targeted-climate scenario SSP2-4.5.

Geoengineering reduces wildfire occurrence through decreasing surface temperature and wind speed and increasing relative humidity and soil water, with the exception of boreal regions where geoengineering increases the occurrence of wildfires due to a decrease in relative humidity and soil water compared to present day. This leads to a global reduction in burned area and fire carbon emissions by the end of the century relative to their base-climate scenario SSP5-8.5. However, geoengineering also yields reductions in precipitation compared to a warming climate, which offsets some of the fire reduction. Overall, the impacts of the different driving factors are larger on burned area than fire carbon emissions. In general, the stratospheric sulfate aerosol approach has a stronger fire-reducing effect than the solar irradiance reduction approach.

1. Introduction

Fire is an important component of the Earth system. It directly impacts climate in two main ways. First, the burning of biomass is one of the major sources of radiatively and/or chemically active trace gases and aerosols in the atmosphere (Andreae and Merlet, 2001; Li et al. 2022). Second, fires pose alterations to terrestrial ecosystem states and functioning such as changing vegetation distribution and structure, disturbing the carbon cycle and water cycle, and changing surface albedo (Bowman et al., 2009; Li and Lawrence, 2017; Liu et al., 2019; Lasslop et al. 2020). In addition to the impact on climate, fires also have significant impacts on air quality and weather across spatial scales (e.g., Bowman et al., 2009, Tang et al., 2022). For example, fires degrade air quality and human health as many of the emitted gases and aerosols from fires are primary pollutants or precursors to secondary chemically-produced pollutants (Wiedinmyer et al., 2006; van der Werf et al., 2006). Fires also alter regional dynamics and weather through changing surface heat and water vapor fluxes, convection, clouds, and precipitation (e.g., Bowman et al., 2009; Coen et al., 2013, Zhang et al., 2022).

Fire is regulated by various factors, including weather and climate conditions (e.g., soil moisture, temperature, precipitation, and wind speed), vegetation composition and structure, and human activities (e.g., land use and land cover change, human ignition and suppression) (e.g., Li et al., 2013; Chen et al., 2017; Knorr et al., 2016a, 2016b; Li et al., 2018; Pechony and Shindell, 2010; van der Werf et al., 2008). These factors also interact with each other in the Earth system (e.g., Walker et al., 2020; Loehman, 2020). For example, climate can alter vegetation composition and structure, and vegetation can also impact climate and weather through evapotranspiration. Due to the complex interactions and feedbacks among these factors and fires, quantifying and projecting the trend of fires is challenging and is subject to large uncertainties. Despite challenges and uncertainties, previous studies have generally suggested that in the future global fire risk will increase, though with significant regional differences (e.g., Abatzoglou et al., 2019; Bowman et al., 2020; Di Virgilio et al., 2019; Flannigan et al., 2009, 2013; Ford et al., 2018; Huang et al., 2015; Li et al., 2020; Liu et al. 2010; Luo et al., 2013; Pechony and Shindell, 2010; Veira et al., 2016). The growing importance combined with large uncertainties of fires has posed an urge to understand and quantify future fire trends in the context of climate change. It has been suggested that future climate mitigation should consider the impact of fires (Shiogama et al., 2020; Ward et al., 2012).

The Shared Socioeconomic Pathways (SSPs) were established to facilitate the integrated analysis of future climate impacts, vulnerabilities, adaptation, and mitigation (Riahi et al., 2017). These SSP scenarios utilized in Phase 6 of the Coupled Model Intercomparison Project (CMIP6) were generated with integrated assessment models, based on five narratives describing alternative socio-economic developments, including sustainable development (SSP1), middle-of-the-road development (SSP2), regional rivalry (SSP3), inequality (SSP4), and fossil-fueled development (SSP5). Different scenarios have different energy, land use, and emissions implications. Corresponding global population projections consistent with each of the SSPs have also been established (Jones and O'Neill, 2016).

Solar geoengineering, also known as solar radiation modification (SRM) or more generally as climate intervention, has been researched as a potential option to offset some of the radiative effects of increasing anthropogenic greenhouse gases in the future through solar radiation

modification (e.g., Kravitz et al., 2015; Tilmes et al., 2009, 2020). One proposed approach is to inject the precursor of sulfate aerosols (sulfur dioxide; SO_2) to the stratosphere that can reflect incoming solar radiation. To understand the impacts of sulfate aerosols compared to direct solar irradiance reduction, both experiments have been performed in parallel (e.g., Xia et al, 2016, Visioni et al., 2021a). Previous studies have analyzed the impact of geoengineering on climate outcomes (e.g., Tilmes et al., 2013, 2020; Visioni et al., 2021a). While global surface temperature targets could be reached, SRM approaches tend to overcompensate the hydrological cycle, with potential consequences to other impacts on climate and the Earth system (e.g., Bala et al., 2008; Tilmes et al., 2013; Lee et al., 2020). Since fire is a key component of the Earth system and the drivers of fires are directly or indirectly changed by solar geoengineering, the impacts of solar geoengineering on fires should also be considered when designing and assessing solar geoengineering approaches.

Deleted: Robock, 2020

In this paper, we use a fully coupled Earth system model CESM2 with WACCM6 as the atmospheric component. CESM2 (WACCM6) is coupled to the Community Land Model (CLM) that includes a prognostic fire scheme, which interacts with various land and atmospheric processes. WACCM6 is currently not using biomass burning emissions derived from the land model. A coupling of fire emissions to the atmosphere would allow to identify additional climate feedback including changes to climate and the vegetation. However, while this feedback is missing, the fire model still responds to changes in the land and atmosphere and is therefore suited to investigate how fires change in the 21st century. We analyze the future trends of burned area and fire carbon emissions under the two geoengineering scenarios and SSP scenarios, and then analyze how the two solar geoengineering approaches impact fire activity. This paper is organized as follows: Section 2 describes the model simulations; Section 3 presents the future trends of burned area and fire carbon emissions under SSP scenarios and geoengineering scenarios. Section 4 discusses how geoengineering impacts fire, and Section 5 concludes the study.

2. Model descriptions and simulations

2.1 CESM2 (WACCM6)

CESM2 (WACCM6) is a community model that has components of ocean, atmosphere, land, sea-ice, land-ice, river, and wave models. These components are coupled in CESM2 by exchanging states and fluxes via a coupler (Danabasoglu et al., 2019). The Community Land Model Version 5 (CLM5) is the land component of CESM2 (Lawrence et al., 2019). CLM uses prescribed temporal land use and land cover change (LULCC), which consists of an annual time series of the spatial distribution of the naturally vegetated and cropland units of each grid cell, combined with the distribution of plant functional types (PFTs) and crop functional types (CFTs) existing in those land units (Lawrence et al., 2019). The interactive fire scheme in the CLM5 is a key component of this study and is described in more detail in Section 2.2. WACCM6 is a high-top atmospheric model with 70 vertical levels and model top at ~140 km, therefore it has reasonable representation of the stratosphere. The default horizontal resolution of WACCM6 is 1.25° × 0.9° (longitude × latitude). WACCM6 also includes comprehensive chemistry and aerosol mechanisms (Gettelman et al., 2019; Emmons et al., 2020, Tilmes et al., 2019).

2.2 Description and evaluation of fire scheme in CESM2/CLM5

The fire scheme in CESM2/CLM5 accounts for four types of fires: agricultural fires in cropland, deforestation fires in the tropical closed forests, peat fires, and non-peat fires outside cropland and tropical closed forests (Li et al., 2012, 2013). Agricultural fire is accounted for in these simulations but is not included in the analysis, since we focus on wildfires here. In the fire scheme, burned area is affected by climate and weather conditions, vegetation composition and structure, and human activities. Climate and weather conditions (e.g., temperature, precipitation, wind, humidity, and soil moisture) impact natural and human ignition and fire spread through fuel availability and fuel combustibility. Human activities impact deforestation fires via deforestation rates that are applied from the Land Use Harmonization dataset (LUH2, Hurtt et al., 2020) that is used in these experiments. Human impacts on non-deforestation and non-peat fires include both ignition and suppression and are parameterized as functions of both population density and Gross Domestic Product (GDP). In our setup, the global population scenarios corresponding to SSP scenarios (Jones and O'Neill, 2016) are used while regionally-explicit GDP was held constant for all WACCM6 simulations analyzed in this study. Fire-induced changes (including biomass and peat burning, vegetation mortality, adjustment of the carbon and nitrogen (C/N) pools, carbon emissions, changes in vegetation structure and functioning as well as surface water and energy fluxes) are then simulated based on the calculated burned area (Li et al., 2012, 2013). These fire-induced surface property changes in the land model further alter atmospheric states (i.e., temperature and water vapor) in the coupled model. Although the burned area and fire carbon emissions are simulated in CLM5, our CESM2/(WACCM6) simulations use prescribed fire emissions based on the CMIP6 projected inventories for trace gases and aerosols (Riahi et al., 2017) for different SSPs and geoengineering scenarios. Changes in fires can have an impact on radiation, precipitation, and therefore vegetation. However, since this paper mainly focuses on the impacts of solar geoengineering on wildfires instead of the other way around, we do not expect the uncoupled fire emissions to have a large impact on our results, but future studies will be needed to further understand the impact. Full coupling of simulated fire aerosol emissions is an area of ongoing development and analysis with the CESM project.

The fire scheme in CESM has been validated and evaluated in both uncoupled and coupled versions (Li et al., 2012, 2013, 2017, 2018; Li and Lawrence 2017) and compared with other fire models within the Fire Modeling Intercomparison Project (FireMIP) (Li et al., 2019). Evaluation results have shown that the fire scheme can reasonably reproduce the observed amount, spatial pattern, seasonality, and interannual variability of global fires, and fire-population relationship under present-day climate, and has a similar historical long-term trend to the multi-source merged historical reconstructions used as input data for CMIP6 (Li et al. 2018, Li et al. 2019). Although the model underestimates the climate impacts on fires in boreal North America, it still performs better than many other fire models (Yue et al., 2016). Here we briefly evaluate the fire carbon emissions from the CESM2 (WACCM6) simulations with two satellite-based fire emission inventories, namely FINNv2.5 (Fire INventory from NCAR Version 2.5; Wiedinmyer et al., 2022) and GFED4.1s (Global Fire Emissions Database, Version 4.1s; Randerson et al., 2018). The annual total emissions and global distributions of WACCM simulations agree well with those from FINNv2.5 and GFED4.1s (Figures S1 and S2). The annual total fire carbon emissions during 2015-2019 estimated from the WACCM simulations (2.5 PgC/yr) fall into the range of GFED4.1s (2.0 PgC/yr) and FINNv2.5 (3.8 PgC/yr).

2.3 SSPs and geoengineering scenarios

The Scenario Model Intercomparison Project (ScenarioMIP) based on SSPs is the primary activity within CMIP6 that provides multi-model climate projections based on alternative scenarios (O'Neill et al., 2016). These climate projections are driven by SSP scenarios and are related to the Representative Concentration Pathways (RCPs) as described below. The Land Use Model Intercomparison Project (LUMIP) also provides LULCC data for SSPs (Lawrence et al., 2016, Hurtt et al., 2020). In this study, the SSP1-2.6, SSP2-4.5, SSP3-7.0, and SSP5-8.5 scenarios (O'Neill et al., 2016) are shown. (1) SSP1-2.6 (sustainable development) is the low end of the range of future forcing pathways in SSP and updates the RCP2.6 scenario. SSP1 includes substantial land use change, particularly with increasing global forest cover. (2) SSP2-4.5 is a scenario that represents the middle part of the range of future forcing pathways and updates the RCP4.5 scenario. Land use and aerosol changes in SSP2 (middle-of-the-road development) are not extreme relative to other SSPs. (3) SSP3-7.0 is a scenario with both substantial land use changes (particularly decreased global forest cover) and high near-term climate forcers emissions, particularly sulfur dioxide (SO_2). (4) SSP5-8.5 is the unmitigated baseline scenario, representing the high end of the range of future pathways, and updates the RCP8.5 scenario. There is relatively little land-use change in the 21st century in this scenario which leads to slow decline in the rate of deforestation (O'Neill et al., 2017).

The Geoengineering MIP Phase 6 (GeoMIP6) proposed experiments for future projection with geoengineering measures implemented based on ScenarioMIP. In this study we also analyze the response of wildfires under two of the geoengineering experiments – G6Sulfur and G6Solar (Kravitz et al., 2015). Both of these geoengineering scenarios aim to reduce globally-averaged forcing from the ScenarioMIP Tier 1 high-forcing scenario (SSP5-8.5), which averages 8.5 W/m^2 of forcing by 2100, to the medium-forcing scenario (SSP2-4.5), which averages 4.5 W/m^2 of forcing by 2100. The geoengineering scenarios were designed to match the surface temperature of SSP2-4.5. G6Sulfur reduces forcing with stratospheric sulfate aerosols. In G6Sulfur experiment, SO_2, the precursor of stratospheric sulfate aerosol has been continuously injected into the model at 25 km altitude at the Equator with the goal of reducing the magnitude of the net anthropogenic radiative forcing and reaching surface temperatures at SSP2-4.5 levels. G6Solar uses the same setup as G6sulfur, but uses solar irradiance reduction to reduce the magnitude of the net anthropogenic radiative forcing. The reduction of the solar constant in G6Solar and the injected SO_2 in G6Sulfur is determined by a feedback algorithm described in Kravitz et al. (2017) and used in Tilmes et al. (2018, 2020). The feedback algorithm identifies differences in the global mean surface temperature between the simulated and the prescribed target temperature each year and from that calculates required changes in the solar constant or SO_2 injections.

Deleted: Both of these geoengineering scenarios aim to reduce forcing from ScenarioMIP Tier 1 high forcing scenario (SSP5-8.5) to the medium forcing scenario (SSP2-4.5), going from 8.5 to 4.5 Wm^{-2} in 2100.

Deleted: ¶

Deleted: ¶

Formatted: Subscript

2.4 Simulations

In this study we analyze results from fully coupled WACCM6 simulations for future projection under the aforementioned scenarios from GeoMIP and ScenarioMIP. The continuous long-term (2015 to 2100) simulations used in this study provide a continuous picture of future fire changes and allow us to investigate when and how major changes in the fire trends occur. The horizontal resolution for land and atmosphere is 1.25° × 0.9° (longitude × latitude). Multiple simulations (2~5 members) are conducted for each scenario except for the SSP1-2.6 and SSP3-7.0 scenarios (see Table S1 for ensemble sizes). Different ensemble sizes could result in differences in ensemble

spread. To be consistent, for scenarios with multiple simulations, only ensemble means are shown and analyzed. I.e., ensemble means are calculated before any analyses or calculations, and hence a scenario with multiple simulations is treated in the same way as a scenario with only one simulation by only using the mean value of the ensemble members. Comparing results from a single simulation to multi-member averages could introduce potential uncertainties as ensemble mean values are in general different from values from a single member. However, the analyses and comparisons here are as useful as comparing single simulations, if not more, because in our approach we attempted to improve model projection for several scenarios by using ensemble means to replace single simulation values when possible. However, the analyses and comparisons here are as useful as comparing single simulations, if not more. The future projection simulations analyzed in this study were initialized with the ensemble WACCM6 historical simulations. Therefore, the initial conditions of different ensemble members are different. Future climate under these simulations has been analyzed in Meehl et al. (2020) and Jones et al. (2020).

3 Future trends of fires

3.1 Future trends of burned area and fire carbon emissions under the SSP scenarios

The global total wildfire burned area in these simulations is projected to increase under all the SSP scenarios (Figure 1a). The largest increases (averages for the 2091-2100 period relative to the 2021-2030 period) in the global burned area are seen in the SSP5-8.5 scenarios (~20%). The changes in SSP1-2.6 and SSP2-4.5 are less than 4% (see Table S2 for projected regional and global change of burned area and fire carbon emissions in 2091-2100 relative to 2021-2030 (%) under different scenarios). In terms of the spatial distribution, the 40°N–70°N latitude is the only latitude band in which the burned area consistently increases under all the SSP scenarios (Figure 1b). In the 10°S–5°N latitude band (tropical region), the burned area consistently decreases under all scenarios to a diverse extent. While global total burned area is expected to increase under most global warming scenarios, burned area may decrease in some regions due to changes in anthropogenic activities or reduced 2-m relative humidity and/or reduced soil moisture. A more detailed discussion on future trends of fire activity under the SSP scenarios are provided in the Supplement.

3.2 Future trends of burned area and fire carbon emissions with geoengineering

The two geoengineering scenarios (G6Sulfur and G6Solar) are based on SSP5-8.5 and targeted SSP2-4.5. As G6Sulfur reduces the forcing through stratospheric sulfate aerosols while G6Solar directly decreases total incoming solar irradiance, the difference between the two provides insight on the other impacts of sulfate aerosols on fires besides the forcing change. Even though fire carbon emissions are largely driven by burned area, they are also impacted by fuel availability and combustion completeness. Therefore, the fire carbon emissions generally show trends consistent with burned area, with some notable differences. Both burned area and fire carbon emissions under the two geoengineering scenarios are lower than those under SSP5-8.5 (Figures 2a and 2c). Lower fire activity in these geoengineering scenarios than SSP5-8.5 is expected due to reduced surface warming towards SSP2-4.5 target climate conditions. However, we found that by the end of the century, the two geoengineering scenarios have lower burned area and fire carbon emissions than not only their base-forcing scenario SSP5-8.5 but also the targeted-forcing scenario SSP2-4.5 (Figures 2a and 2c; see Table S3 for averages of regional and global annual projected

Deleted: WACCM6 historical simulations serve as initial conditions for the future scenarios.

Deleted: The global total wildfire burned area in these simulations is projected to increase under all the SSP scenarios (Figure 1a). The largest increases in the global burned area are seen in the SSP5-8.5 scenarios (~20%) and SSP3-7.0 (~10%). The changes in the other scenarios are relatively small (Table S2). In terms of the spatial distribution, the 40°N–70°N latitude is the only latitude band in which the burned area consistently increases under all the SSP scenarios (Figure 1b). In the 10°S–5°N latitude band (tropical region), the burned area consistently decreases under all scenarios to a diverse extent. A more detailed discussion on future trends of fire activity under the SSP scenarios are provided in the Supplement.

Deleted: and burned area

burned area (Mha/year) and fire carbon emissions in 2091-2100 under different scenarios). The change of the two geoengineering scenarios compared to SSP2-4.5 in the last decade of the century is small in burned area (-2% for G6Solar and -12% for G6Sulfur) but relatively large in fire carbon emissions (-18% for G6Solar and -23% for G6Sulfur). However, when compared to SSP5-8.5, the reduction of the two geoengineering scenarios in burned area (-18% for G6Solar and -26% for G6Sulfur) is similar to that in fire carbon emissions (-20% for G6Solar and -26% for G6Sulfur). This implies that the difference in fire carbon emissions between the two geoengineering scenarios and SSP2-4.5 are less driven by burned area and that fuel availability plays a more important role in this comparison, while for the difference to SSP5-8.5, changes in burned area plays more of a role in emission differences. The two geoengineering approaches (G6solar and G6sulfur) generally lead to reduced fire activity compared to SSP5-8.5 in most regions in 2091-2100, except for Northern Hemisphere Africa and Equatorial Asia (Figures S3 and S4). When comparing the period 2091-2100 to the period 2021-2030, the largest decrease in global total wildfire burned area is seen in the G6sulfur scenario among all the scenarios in this study (~ -11%; see Table S2).

Deleted: by the end

Deleted: –

Deleted: –

Deleted: –

Deleted: –

In the 40°N–70°N latitude band, the burned area consistently increases under not only all the SSP scenarios but also the two geoengineering scenarios when comparing the period 2091-2100 to the period 2021-2030 (Figure 2b). However, the increase in burned area is lower in the two geoengineering scenarios compared to SSP5-8.5 and is similar to the SSP2-45 scenario. In the -20°S–0° latitude band, the reduction in burned area is larger under G6sulfur than that under G6Solar (Figure 2a). Generally, G6sulfur has a stronger fire-reducing effect than G6solar, with exceptions such as over Europe. We also found notable differences between the two geoengineering methods for some specific regions, implying that the geoengineering method chosen could be inequitable for some countries. For example, G6Solar is the better choice for producing less burned area in Europe, while over Southern Hemisphere Africa, G6Sulfur is better than G6Solar (see Figure S4).

4 Mechanism of geoengineering impacting fires

The two SSP5-8.5-based geoengineering scenarios successfully reduce the radiative forcing from 8.5 Wm^{-2} (as in SSP5-8.5) to 4.5 Wm^{-2} (as in SSP2-4.5) in 2100 and global surface temperatures between SSP2-4.5 and the two geoengineering scenarios are nearly the same. However, both geoengineering scenarios produce less fire than SSP2-4.5 by 2100 (Figures 2 and 3). There are different processes involved in the cooling in G6Sulfur (due to the stratospheric sulfate aerosols) and the cooling in G6Solar (due to directly reduced insolation) (Visioni et al., 2021a). Because of the difference in the resulting climate response, these two geoengineering approaches impact fires differently, even though they are designed to achieve the same forcing level by 2100. Previous studies indicate that stratospheric heating caused by aerosols can impact precipitation and temperature at the surface through alterations to stratospheric dynamics (Jiang et al., 2019; Simpson et al., 2019; Richter et al., 2017; Visioni et al., 2020). Last but not least, the two geoengineering approaches also result in different outcomes for other quantities important for fires. For example, enhanced stratospheric aerosol burden results in changes in direct to diffuse light which promotes plant growth (e.g., Xia et al., 2017; Xu et al., 2020). On the other hand, it can reduce in the hydrological cycle and regional precipitation changes due to the aerosol heating effects in the lower tropical stratosphere (e.g., Tilmes et al., 2013, Simpson et al., 2019).

Here we analyze the key variables in the Earth system that are involved in the processes from the reduced insolation on the top of the atmosphere and sulfate aerosols in the stratosphere to fires at the surface. Note that hereafter for a scenario with multiple ensemble members, only the ensemble mean is analyzed and shown. The key variables shown in this section are selected via comparing the key variables that determine fire activity in the fire scheme in CESM2/CLM5 with the key climate variables that are impacted by geoengineering approaches. The analyses are conducted for 14 individual fire regions following Giglio et al. (2010), namely Boreal North America, Temperate North America, Central America, Northern Hemisphere South America, Southern Hemisphere South America, Europe, Middle East, Northern Hemisphere Africa, Southern Hemisphere Africa, Boreal Asia, Central Asia, Southeast Asia, Equatorial Asia, and Australia and New Zealand (Figure S3).

4.1 Surface temperature

Even though the mean surface temperature (TS) for the whole globe and the land are similar under the two geoengineering scenarios and SSP2-4.5 (Figure 4), regional differences exist (Figures 5). For example, over Equatorial Asia, the annual surface mean temperatures in the two geoengineering scenarios are consistently lower than that in SSP2-4.5 by ~0.3K during 2091-2100 (Figure S6). The spatial distribution of burned area difference and fire carbon emission difference between G6Solar/G6Sulfur and SSP5-8.5 (Figure 3) are not always co-located with their spatial distribution of surface temperature difference (Figure 5). To understand to what extent the surface temperature drives fire activity change, we calculate correlations of surface temperature change and burned area/fire carbon emission change for individual fire regions under SSP2-4.5, G6Solar, and G6Sulfur. Surface temperature change (ΔTS) for a given region is calculated based on the individual model grids within the region and annual values between 2091-2100. It is defined as the difference between the analyzed scenario (i.e., G6Solar, G6Sulfur, and SSP2-4.5) and the reference scenario (i.e., SSP5-8.5). Burned area change (ΔBA) and fire carbon emission change (ΔCemis) are defined in the same way. For example, if a region consists of 500 individual model grids, as we use 10 years of annual data, there will be 5000 (500 × 10) pairs of ΔTS and ΔBA to calculate correlations. The correlations calculated here account for spatial variability within the region and interannual variability during 2091-2100.

Overall, surface temperature plays a more important role in the decrease of fire activity in the two geoengineering scenarios compared to that in SSP2-4.5 relative to SSP5-8.5 (Figure 6). This is expected because the only difference between the two geoengineering scenarios and SSP5-8.5 is the specific application of climate intervention; whereas the differences between SSP2-4.5 and SSP5-8.5 involves several other differences including population growth and LULCC. For G6Solar and G6Sulfur, the strongest impact of surface temperature change on burned area occurs over Southern Hemisphere South America (correlation=0.42 for G6Solar and 0.45 for G6Sulfur), followed by Southern Hemisphere Africa, Temperate North America, and Europe. The impact of surface temperature change over boreal regions (Boreal North America and Boreal Asia) are relatively small. This suggests that the changes in area burnt in these regions might be predominantly driven by other factors changed by geoengineering (e.g., hydrological cycle) rather than the surface temperature changes, which will be analyzed in the following sub-sections. For G6Solar and G6Sulfur, the impact of surface temperature on burned area is generally larger than its impact on fire carbon emissions. This is expected as fire carbon emissions in CESM2/WACCM6 are determined by burned area together with vegetation characteristics (carbon

Deleted: This suggests that the changes in area burnt in these regions are not predominantly driven by the surface temperature changes, but by other factors

density and combustion completeness; Li et al., 2012), which introduces more uncertainties. The only exception occurs over the Northern Hemisphere South America where surface temperature plays a more important role in fire carbon emissions than burned area for not only G6Solar (correlation is 0.37 versus 0.29) and G6Sulfur (correlation is 0.37 versus 0.24) but also SSP2-4.5 (correlation is 0.40 versus 0.23). Over Northern Hemisphere South America, the correlations between ΔTS and ΔBA/ΔCemis are also close under the three scenarios. Since combustion completeness is a fixed parameter, this difference points to the possibility that the reduced surface temperature has a larger impact on carbon density over Northern Hemisphere South America than over other regions.

Overall, we find that the surface temperature change introduced by the two geoengineering approaches (solar irradiance reduction and stratospheric sulfate aerosols) by the end of the century impacts burned area and fire carbon emissions, e.g., the introduced cooling results in smaller fire activity. The degree of impact varies dramatically across different regions. The impact of surface temperature in G6Solar and G6Sulfur are overall close. However, surface temperature alone does not account for all the changes in fire activity.

4.2 Precipitation

Precipitation change is also an important consequence of climate change and geoengineering (Figure 4). Global precipitation is expected to increase under climate change as higher tropospheric temperature leads to more moisture in the air. Previous studies found that geoengineering could eliminate these increases in precipitation and can even reduce global mean or regional precipitation relative to the target scenario, depending on the geoengineering approach (Tilmes et al., 2013, Simpson et al., 2019, Visioni et al., 2021a). The spatial distribution of precipitation changes under G6Solar and G6Sulfur relative to SSP5-8.5 are similar (Figure 5). The trend of precipitation varies dramatically across regions (Figure S7). Precipitation is also important for fires. Precipitation itself could have either a positive or a negative impact on future fires because precipitation can impact both fuel combustibility and fuel availability, which impact fire in opposite directions. In addition, precipitation changes can also lead to changes in relative humidity and soil water content, which are important factors for fires. Here we apply the same analyses for precipitation change (ΔPrecip) as in Section 4.1 for surface temperature change (ΔTS).

Deleted: 8

The reduction in precipitation by geoengineering has the opposite impact on fire as the reduction in surface temperature by geoengineering, as shown by the negative correlations of ΔPrecip and ΔBA/ΔCemis (Figure 6). The correlations are consistently negative across all the scenarios (G6Solar, G6Sulfur, and SSP2-4.5) and almost all regions. The largest impact of precipitation change occurs over Equatorial Asia for all three scenarios (correlation is -0.45–-0.42 for ΔBA and -0.43–-0.33 for ΔCemis), which is aligned with the strong precipitation change over the region (Figures 5). Over the Middle East, precipitation change has a relatively large impact on burned area and fire carbon emissions under G6Solar as well as SSP2-4.5, however the impact is small under G6Sulfur. We note that unlike the impact of ΔTS, the impact ΔPrecip is relatively large over boreal regions. We conduct a sensitivity test of 1-year lag correlation (see Table S4 for the correlation values) to understand the impact of previous year precipitation change on fire activity (for example calculating correlation of ΔPrecip for 2091 and ΔBA/ΔCemis for 2092). We found that this correlation is still significant for most regions, though it is generally lower. Overall precipitation change is inversely related to burned area change and fire carbon emission change.

Therefore, for these regions where precipitation is reduced compared to SSP5-8.5 as a consequence of geoengineering such as Equatorial Asia, the reduction in burned area and fire carbon emissions due to reduced surface temperature are offset to some extent.

4.3 Humidity

Humidity is also impacted by geoengineering. The future trends of specific humidity (g/kg) and relative humidity (%) are opposite as specific humidity is projected to increase while relative humidity is projected to decrease compared to SSP5-8.5 (Figure 4). Their spatial distribution and inter-scenario differences are also divergent (Figures 4 and 5). This is due to the fact that relative humidity is driven by not only the actual moisture content but also the temperature. The same amount of water vapor results in a higher relative humidity in colder air than in warm air. Therefore a reduction in relative humidity in a warming climate indicates that the relative amount of water vapor has not increased proportional to the warming. Relative humidity is a driving variable in the CLM5 fire module in multiple places (e.g., lower relative humidity leads to higher fuel combustibility and larger fire spread). Here we focus our analysis on the relative humidity change at 2-meter (ΔRH) as relative humidity is directly used in the CLM5 fire module. Changes in relative humidity show different spatial distribution between the G6solar minus SSP5-8.5 and G6sulfur minus SSP5-8.5 (Figure 5), even though their global average values are close (Figure 4).

Deleted: Since 2-meter relative humidity is strongly driven by evapotranspiration, the difference between G6sulfur and G6Solar points to the possibility that stratospheric sulfate aerosols lead to more scattered light and hence enhanced plant growth than the solar case, which results in more evapotranspiration.

The relative humidity change (ΔRH) is negatively correlated to ΔBA/ΔCemis across all scenarios and regions (Figure 6). Therefore, the higher relative humidity in G6Solar, G6Sulfur, and SSP2-4.5 than SSP5-8.5 (Figure 4) leads to less fire activity globally. Overall, the relative humidity change is more strongly correlated to ΔBA/ΔCemis, indicating that relative humidity change is a more important driver of fire activity change under geoengineering than surface temperature or precipitation.

4.4 Wind speed

Wind speed is also an important driving factor in fire spread and is also indirectly impacted by geoengineering (Figure 4). In CLM5, wind speed is used in the calculation of fire spread and hence burned area. Wind speed mainly has an indirect impact on fire carbon emissions through burned area. Here we analyze 10-meter wind speed (U10). By the end of the century, SSP2-4.5 has slightly higher U10 than SSP5-8.5, G6Solar has similar U10 as SSP5-8.5, while G6Sulfur has slightly lower U10 than SSP5-8.5 over land (Figure 4). However, the regional difference can be relatively large (Figures 5). G6sulfur and G6solar have significantly different U10 over Southern Hemisphere ocean (Figures 5). However, the difference in U10 between G6solar and G6sulfur over land is relatively small with exceptions such as over Australia and Northern Hemisphere Africa where G6sulfur has lower U10.

Wind speed change has consistently positive correlations with changes in burned area and fire carbon emissions under the two geoengineering scenarios across all analyzed regions (which is not the case for SSP2-4.5, where ΔU10 is negatively correlated ΔBA or ΔCemis over most regions). This indicates that the reduction in wind speed as a byproduct of geoengineering (Figure 4) leads to less fire activity globally. The wind speed reduction is relatively large over South Hemisphere Africa (Figure 5), and the correlations are also high, indicating the wind speed reduction is partially responsible for the reduction in fire activity over South Hemisphere Africa.

4.5 Soil water content

Soil water content is a key driver of fire activity as it impacts fuel combustibility and fire spread. Soil water content is indirectly impacted by the geoengineering approaches through the hydrological cycle. The precipitation changes as a result of geoengineering compared to SSP5-8.5 strongly impacts the soil water content, and the soil water content further drives the relative humidity near the surface through evapotranspiration. We see a much smaller reduction in soil water content in the geoengineering runs compared to SSP2-45. Therefore, the future trends of soil water content (here we use the model variable SOILWATER_10CM, i.e., the soil water content in the top 10 cm (kg/m^2) to evaluate soil moisture) are close to the future trends of relative humidity (Figure 4) globally. However, in the last decade of the century, difference in soil water content among the scenarios is larger than the difference in relative humidity among the scenarios (the difference of the 3 scenarios from SSP5-8.5 are ~1–2% for relative humidity and ~4%–7% for SOILWATER_10CM). Here we include analyses of soil water content not only because it is a very important driver of fire activity but also because the spatial distributions of soil water change (ΔSOILWATER) can be different than relative humidity change in some regions (Figures 5). Overall, similar to precipitation and relative humidity, soil water content change is negatively related to burned area and fire carbon emissions with different spatial distributions (Figure 6). For example, over the boreal regions and Europe, the impact of ΔSOILWATER is smaller than the impact of ΔRH, while over Central Asia it is larger.

4.6 Others

There are other relevant variables that are not analyze in detail here. For example, the reduction in the downwelling solar flux at the surface (ΔFSDS) is a direct consequence of geoengineering (solar irradiance reduction and stratospheric sulfate aerosols). In addition, water vapor content and cloud change as a consequence of geoengineering also impact downwelling solar flux at the surface. We include the analyses of downwelling solar flux in the supplement (Figures S8-S9) as the downwelling solar flux at the surface does not directly determine burned area and fire carbon emissions in the model. The downwelling solar flux at the surface is positively related to burned area and fire carbon emissions. Therefore, the lower downwelling solar flux at the surface than SSP5-8.5 as a result of the geoengineering approaches leads to less fires globally while the higher downwelling solar flux at the surface under SSP2-4.5 than SSP5-8.5 tends to increase fire activity and can offset the overall reduction fires in SSP2-4.5 than SSP5-8.5 to some degree. As another example, vegetation carbon can also impact the total fire carbon emissions and are also impacted by fire activity. However, we do not further analyze the impact of fuel load because geoengineering approaches do not seem to change global total fuel load significantly. The future trend of total vegetation carbon under G6Solar and G6Sulfur are very close to SSP5-8.5, and the three of them are different from SSP2-4.5 as total vegetation carbon is largely driven by CO_2 (Figure 4).

Deleted: 9

Deleted: 10

4.7 G6Sulfur versus G6Solar

Comparisons between G6Sulfur and G6Solar provide insight on the potential impact of stratospheric sulfate aerosols on fires other than the intended climate intervention. In general, using sulfur to create climate control enhances the effect of the solar management on the modeled fire response. While both geoengineering approaches show strongest inverse relationships between fire

parameters and relative humidity and soil moisture, G6Sulfur shows smaller reductions in these climate variables than G6Solar. Globally, G6Sulfur has lower burned area and fire carbon emissions than G6Solar by the end of the century. The differences between G6Sulfur and G6Solar varies regionally (Figures 7a-7b). For example, over most regions, G6Sulfur has less fire activity than G6Solar whereas over Europe, G6Sulfur has more fire activity than G6Solar, which is related to the warming over Northern Eurasia caused by G6Sulfur (Figure 7c) and a positive correlation between BA and surface temperature over Europe. However, we note that two ensemble members may not fully reflect the robust signal. The spatial distributions of differences between G6Sulfur and G6Solar in burned area and fire carbon emissions (Figures 7a-7b) are close to the spatial distributions of difference between G6Sulfur and G6Solar in relative humidity (Figure 7e) and soil water content (Figure 7g). G6Sulfur has higher relative humidity and soil water content over most regions. However, over Europe relative humidity and soil water content in G6Sulfur are lower than those in G6Solar, which is consistent with what has been found in burned area and fire carbon emissions. In addition, over South America, the distribution of difference in relative humidity and soil water content is similar to the distribution of difference in burned area and fire carbon emissions. This indicate that the differences in future fire activity between the two geoengineering approaches is likely driven by relative humidity and soil water content.

A summary of the relationships between ΔBA and the changes in the related variables (ΔTS, ΔPrecip, ΔRH, ΔU10, ΔSOILWATER, and ΔFSDS) for G6Sulfur versus G6Solar is shown in Figure 8 (note that ΔBA as well as Δ of other variables are calculated by the difference of the geoengineering run from the reference case, i.e., SSP5-8.5). Overall, the impacts of these driving variables are similar in the two geoengineering approaches (as the points fall close to the diagonal). However, these variables in general have larger impacts on burned area in G6Solar than in G6Sulfur (as the majority of the points fall in the shaded area where the x-axis value is larger than the y-axis value). It is possible that stratospheric sulfate aerosols could yield to additional changes such as higher diffuse radiation that benefits plant growth, which reduces the correlations of the analyzed factors with fires.

Deleted: This is expected since the climate impacts of solar irradiance reduction (G6Solar) is more direct than that of stratospheric sulfate aerosols (G6Sulfur) and stratospheric sulfate aerosols can yield to additional changes (such as higher diffuse radiation that benefits plant growth). This is consistent with that G6Sulfur has slightly higher total vegetation carbon than G6Solar or SSP5-8.5, even though this difference is relatively small compared to the difference caused by CO_2 (Figure 4g).

4.8 Discussion

The key finding of this study is that fire burned area and emissions are lower in the geoengineering runs than not only SSP5-8.5 but also the target SSP2-4.5 run in CESM2/WACCM6. Here we analyze the key climate variables that are largely and/or directly impacted by the two geoengineering approaches and are important drivers of fires. A summary of the relationships between ΔBA and the change in the related variables (ΔTS, ΔPrecip, ΔRH, ΔU10, ΔSOILWATER, and ΔFSDS) versus the relationships between ΔCemis and the change in the related variables for G6Solar, G6Sulfur, and SSP2-4.5 are shown in Figure 9. The future trends of the analyzed variables and their changes from SSP5-8.5 can be opposite over different regions. However, the directions of impact (i.e., positive or negative correlation) are overall consistent across the 14 fire regions and 3 scenarios. Therefore the dominant factors are also different across regions.

We note that under both geoengineering scenarios, changes in relative humidity, soil water, and downwelling solar flux at the surface all have strongest impacts over Equatorial Asia (as shown by strongest correlations among the 14 regions; Figure 9). Changes in wind speed and precipitation also have relative strong impacts over Equatorial Asia compared to other regions. Overall, Equatorial Asia is the most sensitive to the climate variable changes introduced by both

geoengineering approaches (Figure 9), even though the resulting fire activity changes over Equatorial Asia are not as strong as some other regions (Figure 3) likely due to the relatively weak change in the climate variables (e.g., Figures 5). On the contrary, Boreal North America is not sensitive to most of the climate variable changes introduced by both geoengineering approaches (the correlations are the lowest and close to 0, Figure 9), which is likely the reason why the 40°N–70°N latitude band is the only latitude band in which the zonal mean burned area consistently increases even under the geoengineering scenarios (Figures 1 and 2). Boreal Asia is similar to Boreal North America with the correlations overall being slightly stronger.

For G6Solar and G6Sulfur, the correlations of the shown variables (especially for ΔTS, ΔRH, ΔU10, and ΔFSDS) with burned area are in general stronger than their correlations with fire carbon emissions (as shown by more data points that fall into the shaded area). This is expected because these variables directly impact burned area, whereas fire carbon emissions are determined by both burned area and fuel availability. Fuel availability is further directly or indirectly impacted by many variables including but not limited to the shown ones here. Therefore, the correlations between the shown variables with fire carbon emissions are not as strong as their correlations with burned area. The patterns in G6Solar and G6Sulfur and closer to each other when using SSP2-4.5 as a reference (Figures 6). This is not only because their approaches to reducing forcing from SSP5-8.5 to 4.5 W/m^2 are different, but also because the scenario configuration of SSP2-4.5 is different from SSP5-8.5 and SSP5-8.5-based G6Solar and G6Sulfur (e.g., LULCC).

The analyses above (Sections 4.1-4.7) use SSP5-8.5 as the reference case to calculate the changes (Δ) because the two geoengineering scenarios are based on SSP5-8.5, and their difference is only due to the geoengineering approaches. Here we also include analyses that uses the target SSP2-4.5 as the reference case in the Supplement (Figures S12). The signs of the correlations are in general consistent whether SSP5-8.5 or SSP2-4.5 is used as the reference case (Figures S11-S12). For example, even though relative humidity change from SSP2-4.5 are very different regionally under G6Solar and G6Sulfur (Figure 5), the signs of the correlations are consistently negative over all regions and under the two geoengineering scenarios. In general, the impacts of the analyzed variables on changes of the burned area and fire carbon emissions from SSP2-4.5 are weaker (Figures S11-S12), likely due to the fact that the changes (Δ) between the two geoengineering scenarios and SSP2-4.5 are due to not only geoengineering introduced climate variable changes (e.g., surface temperature, relative humidity, soil water content, etc.) but also other factors such as atmospheric CO_2 and LULCC.

4.9 Uncertainty and limitation

We recognize that there are several limitations in this study. For example, even though CESM2 is a state-of-the-art model, uncertainties and limitations exist in the model parameterizations (including the parameterization of fire-related processes and the lack of interactive fire emissions). In addition, the fire emissions of trace gases and aerosols are not fully coupled, as CESM2 uses the CMIP6 fire emission inventories. This study analyzes results from only one model (CESM2) and similar studies need to be conducted with other models to test inter-model consistency. Lastly, there are only two ensemble members in each geoengineering scenario, which can lead to larger variability at regional scale in particular resulting in large uncertainties in the response of geoengineering on rainfall with implications of other relevant variables. While largescale changes are significant, a larger ensemble size in future study will reduce uncertainties

Deleted: For G6Solar and G6Sulfur, the impacts of the shown variables (especially for ΔTS, ΔRH, ΔU10, and ΔFSDS) on burned area are in general stronger than their impacts on fire carbon emissions (as shown by more data points that fall into the shaded area). This is expected because these variables first impact burned area, and then fire carbon emissions are determined by burned area and fuel availability. Fuel availability is further directly or indirectly impacted by many other variables including the shown ones here, which introduce more uncertainties. The patterns in G6Solar and G6Sulfur and closer to each other when using SSP2-4.5 as a reference (Figures 6). This is not only because their approaches to reducing forcing from SSP5-8.5 to 4.5 W/m^2 are different, but also because the scenario configuration of SSP2-4.5 is different from SSP5-8.5 and SSP5-8.5-based G6Solar and G6Sulfur (e.g., LULCC).¶

Deleted: 3

Deleted: 4

Deleted: 5

Deleted: 4

Deleted: 5

in the regional results. More studies are needed to fully understand the future trends of fires and the impact of geoengineering on fires.

5. Conclusions

Here we analyzed the future fires under geoengineering as well as SSP scenarios, and assess how the different geoengineering approaches impact fires. The major conclusions and implications are as follows:

(1) The global total wildfire burned area is projected to increase under the unmitigated scenario (SSP5-8.5), and decrease under the two geoengineering scenarios (solar irradiance reduction and stratospheric sulfate aerosols) comparing the averages of 2091-2100 relative to 2021-2030.

(2) By the end of the century, the two geoengineering scenarios exhibit lower burned area and fire carbon emissions than not only their base-forcing scenario (SSP5-8.5) but also the targeted-forcing scenario (SSP2-4.5).

(3) The two geoengineering approaches (solar irradiance reduction and stratospheric sulfate aerosols) generally lead to less wildfire activity in most regions in 2091-2100, except for the Northern Hemisphere Africa and Equatorial Asia. The 40°N–70°N latitude band is the only latitude band in which the zonal mean burned area consistently increases under all the scenarios, even the geoengineering scenarios.

(4) Overall, changes of G6Solar and G6Sulfur from SSP5-8.5 in surface temperature, wind speed, and downwelling solar flux at the surface are positively correlated to the changes in burned area and fire carbon emissions, while their changes in precipitation, relative humidity, and soil water content are negatively correlated to the changes in burned area and fire carbon emissions.

(5) Generally, the stratospheric sulfate aerosols approach has a stronger fire-reducing effect than the solar irradiance reduction approach. The impacts of the analyzed variable changes are generally larger (percent-wise) on burned area than fire carbon emissions.

(6) Geoengineering imposed reduction in surface temperature and wind speed, and increase in relative humidity and soil moisture, reduce fires by the end of the century. However, the reduction in precipitation resulting from geoengineering offsets its overall fire-reducing effect to some extent.

The success of future fire mitigation with the two geoengineering approaches in the CESM2/WACCM6 model results is encouraging. However, this study is not a closure study due to the uncertainties and limitations (Section 4.9). More research is needed for this topic. Here we do not indicate that fewer fires under the geoengineering approaches are definitively beneficial. After all, fire is a natural process and a key component of the dynamic Earth system, and wildfires were present long before anthropogenic activities. Lastly, fire risk increase is only one of many possible consequences of climate change, and fire activity reduction is also only one of many possible consequences of climate intervention. We present this study only as a reference for the future when geoengineering is considered.

Data availability

The simulation data used in this study are archived on the Earth System Grid Federation (ESGF) (https://esgf-node.llnl.gov/projects/cmip6; last access: 12 December 2022). The model Source ID is CESM2-WACCM for CESM2-WACCM6. FINN2.5 data are available at:

Deleted: 4

Deleted: in the 21st century

https://www.acom.ucar.edu/Data/fire/. GFED data are available at: https://www.globalfiredata.org/.

Author contributions

WT led the analysis with the contribution from ST. ST and DML contributed to the interpretation of the model results. WT prepared the paper with improvements from ST, DML, FL, CH, LKE, RRB, and LX.

Acknowledgements

This material is based upon work supported by the National Center for Atmospheric Research, which is a major facility sponsored by the National Science Foundation under Cooperative Agreement No. 1852977. W. Tang was supported by NCAR Advanced Study Program Postdoctoral Fellowship. We thank the reviewers for their helpful comments that improves this manuscript. W. Tang thanks Wangcai Bao (Syrian hamster; Sep 8, 2020 – Jul 22, 2022) for his support during the pandemic.

Deleted: Wenfu

References

Abatzoglou, J. T., Williams, A. P., & Barbero, R. (2019). Global emergence of anthropogenic climate change in fire weather indices. Geophysical Research Letters, 46(1), 326-336.

Andela, N. and van der Werf, G.R., 2014. Recent trends in African fires driven by cropland expansion and El Nino to La Nina transition. Nature Climate Change, 4(9), pp.791-795.

Andela N, Morton DC, Giglio L, Chen Y, Van Der Werf GR, Kasibhatla PS, DeFries RS, Collatz GJ, Hantson S, Kloster S, Bachelet D. A human-driven decline in global burned area. Science. 2017 Jun 30;356(6345):1356-62.

Bala, et al. (2008): Impact of geoengineering schemes on the global hydrological cycle, PNAS, doi:10.1073/pnas.0711648105.

Bowman, D.M., Balch, J.K., Artaxo, P., Bond, W.J., Carlson, J.M., Cochrane, M.A., D'Antonio, C.M., DeFries, R.S., Doyle, J.C., Harrison, S.P. and Johnston, F.H., 2009. Fire in the Earth system. science, 324(5926), pp.481-484.

Bowman, D. M. J. S., Balch, J. K., Artaxo, P., Bond, W. J., Carlson, J. M., Cochrane, M. A., D'Antonio, C. M., DeFries, R. S., Doyle, J. C., Harrison, S. P., Johnston, F. H., Keeley, J. E., Ford, B., Val Martin, M., Zelasky, S. E., Fischer, E. V., Anenberg, S. C., Heald, C. L., and Pierce, J. R.: Future Fire Impacts on Smoke Concentrations, Visibility, and Health in the Contiguous United States, GeoHealth, 2, 229–247, 2018.

Bowman, D. M. J. S., Kolden, C. A., Abatzoglou, J. T., Johnston, F. H., van der Werf, G. R., & Flannigan, M. (2020). Vegetation fires in the Anthropocene. Nature Reviews Earth & Environment, 1-16.

Brey, S. J., Barnes, E. A., Pierce, J. R., Wiedinmyer, C., & Fischer, E. V. (2018). Environmental conditions, ignition type, and air quality impacts of wildfires in the southeastern and western United States. Earth's Future, 6(10), 1442-1456.

Brey, S. J., Barnes, E. A., Pierce, J. R., Swann, A. L., & Fischer, E. V. Past variance and future projections of the environmental conditions driving western US summertime wildfire burn area. Earth's Future, e2020EF001645, 2020.

Chen, Y., Morton, D. C., Andela, N., Van Der Werf, G. R., Giglio, L., & Randerson, J. T. (2017). A pan-tropical cascade of fire driven by El Niño/Southern Oscillation. Nature Climate Change, 7(12), 906-911.

Coen, J., Cameron, M., Michalakes, J., Patton, E., Riggan, P., and Yedinak, K.: WRF-Fire: Coupled weather-wildland fire modeling with the Weather Research and Forecasting model, J. Appl. Meteor. Climatol., 52, 16–38, doi:10.1175/JAMC-D-12-023.1, 2013.

Danabasoglu, G., Lamarque, J. F., Bacmeister, J., Bailey, D. A., DuVivier, A. K., Edwards, J., Emmons, L. K., Fasullo, J., Garcia, R., Gettelman, A., Hannay, C., Holland, M. M., Large, W. G., Lauritzen, P. H., Lawrence, D. M., Lenaerts, J. T. M., Lindsay, K., Lipscomb, W. H., Mills, M. J., Neale, R., Oleson, K. W., OttoBliesner, B., Phillips, A. S., Sacks, W., Tilmes, S., van Kampenhout, L., Vertenstein, M., Bertini, A., Dennis, J., Deser, C., Fischer, C., Fox-Kemper, B., Kay, J. E., Kinnison, D., Kushner, P. J., Larson, V. E., Long, M. C., Mickelson, S., Moore, J. K., Nienhouse, E., Polvani, L., Rasch, P. J., and Strand, W. G.: The Community Earth System Model Version 2 (CESM2), J. Adv. Model. Earth Syst., 12, 1–35, https://doi.org/10.1029/2019MS001916, 2020.

Di Virgilio, G., Evans, J. P., Blake, S. A. P., Armstrong, M., Dowdy, A. J., Sharples, J., & McRae, R.: Climate change increases the potential for extreme wildfires. Geophysical Research Letters, 46, 8517–8526. https://doi.org/10.1029/2019GL083699, 2019.

Di Virgilio G, Evans JP, Clarke H, Sharples J, Hirsch AL, Hart MA. Climate change significantly alters future wildfire mitigation opportunities in southeastern Australia. Geophysical Research Letters. 2020 Aug 16;47(15):e2020GL088893.

Emmons, L. K., Schwantes, R. H., Orlando, J. J., Tyndall, G., Kinnison, D., Lamarque, J.-F., Marsh, D., Mills, M. J., Tilmes, S., Bardeen, Ch., Buchholz, R. R., Conley, A., Gettelman, A., Garcia, R., Simpson, I., Blake, D. R., Meinardi, S., and Pétron, G.: The Chemistry Mechanism in the Community Earth System Model version 2 (CESM2), J. Adv. Model. Earth Sys., 12, e2019MS001882, https://doi.org/10.1029/2019MS001882, 2020.

Flannigan M, Campbell I, Wotton M, Carcaillet C, Richard P, Bergeron Y. Future fire in Canada's boreal forest: paleoecology results and general circulation model-regional climate model simulations. Canadian journal of forest research. 2001 May 1;31(5):854-64.

Flannigan, M. D., Krawchuk, M. A., de Groot, W. J. et al.: Implications of changing climate for global wildland fire, Int. J. Wildland Fire, 18, 483–507, 2009.

Flannigan, M., Cantin, A. S., De Groot, W. J., Wotton, M., Newbery, A., & Gowman, L. M.: Global wildland fire season severity in the 21st century. Forest Ecology and Management, 294, 54-61, 2013.

Ford B, Val Martin M, Zelasky SE, Fischer EV, Anenberg SC, Heald CL, Pierce JR. Future fire impacts on smoke concentrations, visibility, and health in the contiguous United States. GeoHealth. 2018 Aug;2(8):229-47.

Gettelman, A., Mills, M. J., Kinnison, D. E., Garcia, R. R., Smith, A. K., Marsh, D. R., Tilmes, S., Vitt, F., Bardeen, C. G., McInerny, J., Liu, H.-L., Solomon, S. C., Polvani, L. M., Emmons, L. K., Lamarque, J.-F., Richter, J. H., Glanville, A. S., Bacmeister, J. T., Phillips, A. S., Neale, R. B.,

753 Simpson, I. R., DuVivier, A. K., Hodzic, A., and Randel, W. J.: The Whole Atmosphere
754 Community Climate Model Version 6 (WACCM6), Journal of Geophysical Research:
755 Atmospheres, https://doi.org/10.1029/2019JD030943, 2019.

756 Girardin MP, Mudelsee M. Past and future changes in Canadian boreal wildfire activity.
757 Ecological Applications. 2008;18(2):391-406.

766 Giglio, L., Randerson, J. T., van der Werf, G. R., Kasibhatla, P. S., Collatz, G. J., Morton, D. C.,
767 and DeFries, R. S.: Assessing variability and long-term trends in burned area by merging multiple
768 satellite fire products, Biogeosciences, 7, 1171–1186, https://doi.org/10.5194/bg-7-1171-2010,
769 2010.

770 Hanes, C. C., Wang, X., Jain, P., Parisien, M. A., Little, J. M., & Flannigan, M. D. (2019). Fire-
771 regime changes in Canada over the last half century. Canadian Journal of Forest Research, 49(3),
772 256-269.

773 Huang Y, Jin Y, Schwartz MW, Thorne JH. Intensified burn severity in California's northern
774 coastal mountains by drier climatic condition. Environmental Research Letters. 2020 Sep
775 25;15(10):104033.

776 Hurtt, G.C., L. Chini. R. Sahajpal, S. Frolking, B.L. Bodirsky, K. Calvin, J.C. Doelman, J. Fisk, S.
777 Fujimori, K.K. Goldewijk, T. Hasegawa, P. Havlik, A. Henimann, F. Humpnoder, J. Jungclaus, J.
778 Kaplan, J. Kennedy, T. Kristzin, D. Lawrence, P. Lawrence, L. Ma, O. Mertz, J. Pongratz, A. Popp,
779 B. Poulter, K. Riahi, E. Shevliakova, E. Stehfest, P. Thornton, F.N. Tubiello, D.P. Van Vuuren,
780 and X. Zhang, 2020. Harmonization of Global Land-Use Change and Management for the Period
781 850-2100 (LUH2) for CMIP6. GMD, 13, 5425-5464, doi.org/10.5194/gmd-13-5425-2020.

782 Jiang, J., Cao, L., MacMartin, D. G., Simpson, I. R., Kravitz, B., Cheng, W., Visioni, D., Tilmes,
783 S., Richter, J. H., and Mills, M. J.: Stratospheric Sulfate Aerosol Geoengineering Could Alter the
784 High-Latitude Seasonal Cycle, Geophys. Res. Lett., 46, 14153–14163,
785 https://doi.org/10.1029/2019GL085758, 2019.

786 Jones, B. and O'Neill, B. C.: Spatially explicit global population scenarios consistent with the
787 Shared Socioeconomic Pathways, Environ. Res. Lett., 11, 4003, https://doi.org/10.1088/1748-
788 9326/11/8/084003, 2016.

789 Jones, A., Haywood, J. M., Jones, A. C., Tilmes, S., Kravitz, B., and Robock, A.: North Atlantic
790 Oscillation response in GeoMIP experiments G6solar and G6sulfur: why detailed modelling is
791 needed for understanding regional implications of solar radiation management, Atmos. Chem.
792 Phys. Discuss., https://doi.org/10.5194/acp-2020-802, in review, 2020.

793 Krawchuk, M. A., Kull, C. A., Marston, J. B., Moritz, M. A., Prentice, I. C., Roos, C. I., Scott,
794 A. C., Swetnam, T. W., van der Werf, G. R., and Pyne, S. J.: Fire in the Earth System, Science,
795 324, 481–484, https://doi.org/10.1126/science.1163886, 2009.

796 Knorr, W., Arneth, A., and Jiang, L.: Demographic controls of future global fire risk, Nat. Clim.
797 Change, 6, 781–785, https://doi.org/10.1038/NCLIMATE2999, 2016a.

798 Knorr, W., Jiang, L., and Arneth, A.: Climate, CO2 and human population impacts on global
799 wildfire emissions, Biogeosciences, 13, 267–282, https://doi.org/10.5194/bg-13-267-2016, 2016b.

800 Kravitz, B., Robock, A., Tilmes, S., Boucher, O., English, J. M., Irvine, P. J., Jones, A., Lawrence,
801 M. G., MacCracken, M., Muri, H., Moore, J. C., Niemeier, U., Phipps, S. J., Sillmann, J.,

Storelvmo, T., Wang, H., and Watanabe, S.: The Geoengineering Model Intercomparison Project Phase 6 (GeoMIP6): simulation design and preliminary results, Geosci. Model Dev., 8, 3379-3392, doi:10.5194/gmd-8-3379-2015, 2015.

Kravitz, B., Lamarque, J.-F., Tribbia, J. J., Tilmes, S., Vitt, F., Richter, J. H., MacMartin, D. G., and Mills, M. J.: First Simulations of Designing Stratospheric Sulfate Aerosol Geoengineering to Meet Multiple Simultaneous Climate Objectives, J. Geophys. Res.-Atmos., 122, 12616–12634, https://doi.org/10.1002/2017jd026874, 2017.

Lasslop, G., Hantson, S., Harrison, S. P., Bachelet, D., Burton, C., Forkel, M., Forrest, M., Li F., Melton, J. R., Yue, C., Archibald, S., Scheiter, S., Arneth, A., Hickler, T., and Sitch, S.: Global ecosystems and fire: Multi-model assessment of fire-induced tree-cover and carbon storage reduction, Glob. Change Biol., 26, 5027–5041, https://doi.org/10.1111/gcb.15160, 2020.

Lawrence, D. M., Hurtt, G. C., Arneth, A., Brovkin, V., Calvin, K. V., Jones, A. D., Jones, C. D., Lawrence, P. J., de Noblet-Ducoudré, N., Pongratz, J., Seneviratne, S. I., and Shevliakova, E.: The Land Use Model Intercomparison Project (LUMIP) contribution to CMIP6: rationale and experimental design, Geosci. Model Dev., 9, 2973–2998, https://doi.org/10.5194/gmd-9-2973-2016, 2016.

Lawrence, D. M., Fisher, R. A., Koven, C. D., Oleson, K. W., Swenson, S. C., Bonan, G., Collier, N., Ghimire, B., van Kampenhout, L., Kennedy, D., Kluzek, E., Lawrence, P. J., Li, F., Li, H., Lombardozzi, D., Riley, W. J., Sacks, W. J., Shi, M., Vertenstein, M., Wieder, W. R., Xu, C., Ali, A. A., Badger, A. M., Bisht, G., Brunke, M. A., Burns, S. P., Buzan, J., Clark, M., Craig, A., Dahlin, K., Drewniak, B., Fisher, J. B., Flanner, M., Fox, A. M., Gentine, P., Hoffman, F., Keppel-Aleks, G., Knox, R., Kumar, S., Lenaerts, J., Leung, L. R., Lipscomb, W. H., Lu, Y., Pandey, A., Pelletier, J. D., Perket, J., Randerson, J. T., Ricciuto, D. M., Sanderson, B. M., Slater, A., Subin, Z. M., Tang, J., Thomas, R. Q., Val Martin, M., and Zeng, X.: The Community Land Model version 5: Description of new features, benchmarking, and impact of forcing uncertainty. Journal of Advances in Modeling Earth Systems, 11(12), 4245-4287, 2019.

Le Goff H, Flannigan MD, Bergeron Y. Potential changes in monthly fire risk in the eastern Canadian boreal forest under future climate change. Canadian journal of forest research. 2009 Dec;39(12):2369-80.

Lee, et al. (2020): Expanding the design space of stratospheric aerosol geoengineering to include precipitation-based metrics and explore trade-offs, Earth System Dynamics, doi:10.5194/esd-11-1051-2020.

Li, F., Zeng, X. D., and Levis, S.: A process-based fire parameterization of intermediate complexity in a Dynamic Global Vegetation Model, Biogeosciences, 9, 2761–2780, https://doi.org/10.5194/bg-9-2761-2012, 2012.

Li, F., Levis, S., and Ward, D. S.: Quantifying the role of fire in the Earth system – Part 1: Improved global fire modeling in the Community Earth System Model (CESM1), Biogeosciences, 10, 2293–2314, https://doi.org/10.5194/bg-10-2293-2013, 2013.

Li, F. and Lawrence, D. M.: Role of fire in the global land water budget during the 20th century through changing ecosystems, J. Climate, 30, 1893–908, 2017.

Li, F., Lawrence, D. M., and Bond-Lamberty, B.: Impact of fire on global land surface air temperature and energy budget for the 20th century due to changes within ecosystems, Environ. Res. Lett., 12, https://doi.org/10.1088/1748-9326/aa6685, 2017.

Li, F., Lawrence, D. M., and Bond-Lamberty, B.: Human impacts on 20th century fire dynamics and implications for global carbon and water trajectories, Global Planet. Change, 162, 18–27, 2018.

Li, F., Val Martin, M., Andreae, M. O., Arneth, A., Hantson, S., Kaiser, J. W., Lasslop, G., Yue, C., Bachelet, D., Forrest, M., Kluzek, E., Liu, X., Mangeon, S., Melton, J. R., Ward, D. S., Darmenov, A., Hickler, T., Ichoku, C., Magi, B. I., Sitch, S., van der Werf, G. R., Wiedinmyer, C., and Rabin, S. S.: Historical (1700–2012) global multi-model estimates of the fire emissions from the Fire Modeling Intercomparison Project (FireMIP), Atmos. Chem. Phys., 19, 12545–12567, https://doi.org/10.5194/acp-19-12545-2019, 2019.

Li, Y., Mickley, L. J., Liu, P., and Kaplan, J. O.: Trends and spatial shifts in lightning fires and smoke concentrations in response to 21st century climate over the national forests and parks of the western United States, Atmos. Chem. Phys., 20, 8827–8838, https://doi.org/10.5194/acp-20-8827-2020, 2020.

Li F., D. Lawrence, Y.-Q. Jiang, X.-H. Liu, and Z.-D. Lin, 2022: Fire aerosols slow down the global water cycle, J. Climate, https://journals.ametsoc.org/view/journals/clim/aop/JCLI-D-21-0817.1/JCLI-D-21-0817.1.xml.

Liu, Y. Q., Stanturf, J., and Goodrick, S.: Trends in global wildfire potential in a changing climate, Forest Ecol. Manag., 259, 685–697, https://doi.org/10.1016/j.foreco.2009.09.002, 2010.

Liu, Z., Ballantyne, A. P., & Cooper, L. A. (2019). Biophysical feedback of global forest fires on surface temperature. Nature communications, 10(1), 1-9.

Loehman, R. A. (2020). Drivers of wildfire carbon emissions. Nature Climate Change, 1-2.

Luo, L. F., Tang, Y., Zhong, S. Y., Bian, X. D., and Heilman, W. E.: Will Future Climate Favor More Erratic Wildfires in the Western United States?, J. Appl. Meteorol. Climatol., 52, 2410–2417, https://doi.org/10.1175/jamc-d-12-0317.1, 2013.

Meehl, G. A., Arblaster, J. M.,Bates, S., Richter, J. H., Tebaldi, C.,Gettelman, A., et al. (2020).Characteristics of future warm er basestates in CESM2. Earth and Sp aceScience, 7, e2020EA001296. https://doi.org/10.1029/2020EA001296.

Riahi, K., van Vuuren, D. P., Kriegler, E., Edmonds, J., O'Neill, B. C., Fujimori, S., Bauer, N., Calvin, K., Dellink, R., Fricko, O., Lutz, W., Popp, A., Cuaresma, J. C., KC, S., Leimbach, M., Jiang, L., Kram, T., Rao, S., Emmerling, J., Ebi, K., Hasegawa, T., Havlik, P., Humpenöder, F., Da Silva, L. A., Smith, S., Stehfest, E., Bosetti, V., Eom, J., Gernaat, D., Masui, T., Rogelj, J., Strefler, J., Drouet, L., Krey, V., Luderer, G., Harmsen, M., Takahashi, K., Baumstark, L., Doelman, J. C., Kainuma, M., Klimont, Z., Marangoni, G., Lotze-Campen, H., Obersteiner, M., Tabeau, A., and Tavoni, M.: The Shared Socioeconomic Path ways and their energy, land use, and greenhouse gas emissions implications: An overview, Global Environ. Chang., 42, 153– 168, https://doi.org/10.1016/j.gloenvcha.2016.05.009, 2017.

Richter, J. H., Tilmes, S., Mills, M. J., Tribbia, J. J., Kravitz, B., Macmartin, D. G., Vitt, F., and Lamarque, J. F.: Stratospheric dynamical response and ozone feedbacks in the presence of SO2

injections, J. Geophys. Res.-Atmos., 122, 12557–12573, https://doi.org/10.1002/2017JD026912, 2017.

O'Neill, B. C., Tebaldi, C., van Vuuren, D. P., Eyring, V., Friedlingstein, P., Hurtt, G., Knutti, R., Kriegler, E., Lamarque, J.-F., Lowe, J., Meehl, G. A., Moss, R., Riahi, K., and Sanderson, B. M.: The Scenario Model Intercomparison Project (ScenarioMIP) for CMIP6, Geosci. Model Dev., 9, 3461–3482, https://doi.org/10.5194/gmd-9-3461-2016, 2016.

O'Neill BC, Kriegler E, Ebi KL, Kemp-Benedict E, Riahi K, Rothman DS, van Ruijven BJ, van Vuuren DP, Birkmann J, Kok K, Levy M. The roads ahead: Narratives for shared socioeconomic pathways describing world futures in the 21st century. Global environmental change. 2017 Jan 1;42:169-80.

Pechony, O. and Shindell, D.: Driving forces of global wildfires over the past millennium and the forthcoming century, P. Natl. Acad. Sci. USA, 107, 19167–19170, doi:10.1073/pnas.1003669107, 2010.

Pitman AJ, Narisma GT, McAneney J. The impact of climate change on the risk of forest and grassland fires in Australia. Climatic Change. 2007 Oct 1;84(3-4):383-401.

Randerson, J.T., G.R. van der Werf, L. Giglio, G.J. Collatz, and P.S. Kasibhatla. 2018. Global Fire Emissions Database, Version 4.1 (GFEDv4). ORNL DAAC, Oak Ridge, Tennessee, USA. https://doi.org/10.3334/ORNLDAAC/1293.

Rey, D. M., Walvoord, M. A., Minsley, B. J., Ebel, B. A., Voss, C. I., & Singha, K. (2020). Wildfire-Initiated Talik development exceeds current thaw projections: Observations and models from Alaska's continuous permafrost zone. Geophysical Research Letters, 47, e2020GL087565. https://doi.org/10.1029/2020GL087565.

Shiogama, H., Hirata, R., Hasegawa, T., Fujimori, S., Ishizaki, N. N., Chatani, S., Watanabe, M., Mitchell, D., and Lo, Y. T. E.: Historical and future anthropogenic warming effects on droughts, fires and fire emissions of CO2 and PM2.5 in equatorial Asia when 2015-like El Niño events occur, Earth Syst. Dynam., 11, 435–445, https://doi.org/10.5194/esd-11-435-2020, 2020.

Simpson, I., Tilmes, S., Richter, J., Kravitz, B., MacMartin, D., Mills, M., Fasullo, J., and Pendergrass, A.: The regional hydroclimate response to stratospheric sulfate geoengineering and the role of stratospheric heating, J. Geophys. Res.-Atmos., 124, 2019JD031093, https://doi.org/10.1029/2019JD031093, 2019.

Stralberg D, Wang X, Parisien MA, Robinne FN, Sólymos P, Mahon CL, Nielsen SE, Bayne EM. Wildfire-mediated vegetation change in boreal forests of Alberta, Canada. Ecosphere. 2018 Mar;9(3):e02156.

Tang et al., Effects of fire diurnal variation and plume rise on U.S. air quality during FIREX-AQ and WE-CAN based on the Multi-Scale Infrastructure for Chemistry and Aerosols (MUSICAv0), JGR-Atmosphere, 2022, https://doi.org/10.1029/2022JD036650.

Tilmes, S., Garcia, R. R., Kinnison, D. E., Gettelman, A., and Rasch, P. J.: Impact of geoengineered aerosols on the troposphere and stratosphere, J. Geophys. Res., 114, D12305, https://doi.org/10.1029/2008JD011420, 2009.

Deleted: Robock A. Benefits and risks of stratospheric solar radiation management for climate intervention (geoengineering). Bridge. 2020 Mar 1;50(1):59-67.¶

924 Tilmes S, Fasullo J, Lamarque JF, Marsh DR, Mills M, Alterskjær K, Muri H, Kristjánsson JE,
925 Boucher O, Schulz M, Cole JN. The hydrological impact of geoengineering in the Geoengineering
926 Model Intercomparison Project (GeoMIP). Journal of Geophysical Research: Atmospheres. 2013
927 Oct 16;118(19):11-036.

928 Tilmes, S., Richter, J. H., Kravitz, B., Macmartin, D. G., Mills, M. J., Simpson, I. R., Glanville, A.
929 S., Fasullo, J. T., Phillips, A. S., Lamarque, J. F., Tribbia, J., Edwards, J., Mickelson, S., and Ghosh,
930 S.: CESM1(WACCM) stratospheric aerosol geoengineering large ensemble project, B. Am.
931 Meteorol. Soc., 99, 2361– 2371, https://doi.org/10.1175/BAMS-D-17-0267.1, 2018.

932 Tilmes, S., Hodzic, A., Emmons, L. K., Mills, M. J., Gettelman, A., Kinnison, D. E., ... &
933 Campuzano-Jost, P. (2019). Climate forcing and trends of organic aerosols in the Community
934 Earth System Model (CESM2). Journal of Advances in Modeling Earth Systems, 11(12), 4323-
935 4351.

936 Tilmes, S., MacMartin, D. G., Lenaerts, J. T. M., van Kampenhout, L., Muntjewerf, L., Xia, L.,
937 Harrison, C. S., Krumhardt, K. M., Mills, M. J., Kravitz, B., and Robock, A.: Reaching 1.5 and
938 2.0 °C global surface temperature targets using stratospheric aerosol geoengineering, Earth Syst.
939 Dynam., 11, 579– 601, https://doi.org/10.5194/esd-11-579-2020, 2020.

940 Tilmes, S., MacMartin, D. G., Lenaerts, J. T. M., van Kampenhout, L., Muntjewerf, L., Xia, L.,
941 Harrison, C. S., Krumhardt, K. M., Mills, M. J., Kravitz, B., and Robock, A.: Reaching 1.5 and
942 2.0 °C global surface temperature targets using stratospheric aerosol geoengineering, Earth Syst.
943 Dynam., 11, 579–601, https://doi.org/10.5194/esd-11-579-2020, 2020.

944 Val Martin, M., Heald, C. L., Lamarque, J.-F., Tilmes, S., Emmons, L. K., and Schichtel, B. A.:
945 How emissions, climate, and land use change will impact mid-century air quality over the United
946 States: a focus on effects at national parks, Atmos. Chem. Phys., 15, 2805–2823,
947 https://doi.org/10.5194/acp-15-2805-2015, 2015.

948 Veira, A., Lasslop, G., and Kloster, S.: Wildfires in a warmer climate: emission fluxes, emission
949 heights, and black carbon concentrations in 2090–2099, J. Geophys. Res.-Atmos., 121, 3195–
950 3223, 2016.

951 Visioni, D., MacMartin, D. G., Kravitz, B., Lee, W., Simpson, I. R., and Richter, J. H.: Reduced
952 poleward transport due to stratospheric heating under stratospheric aerosols geoengineering,
953 Geophys. Res. Lett., 47, e2020GL089470, https://doi.org/10.1029/2020GL089470, 2020.

954 Visioni, D., MacMartin, D. G., Kravitz, B., Boucher, O., Jones, A., Lurton, T., Martine, M., Mills,
955 M. J., Nabat, P., Niemeier, U., Séférian, R., and Tilmes, S.: Identifying the sources of uncertainty
956 in climate model simulations of solar radiation modification with the G6sulfur and G6solar
957 Geoengineering Model Intercomparison Project (GeoMIP) simulations, Atmos. Chem. Phys., 21,
958 10039–10063, https://doi.org/10.5194/acp-21-10039-2021, 2021a.

959 Visioni D, MacMartin DG, Kravitz B. Is turning down the sun a good proxy for stratospheric
960 sulfate geoengineering?. Journal of Geophysical Research: Atmospheres. Mar
961 16;126(5):e2020JD033952, 2021b.

962 van der Werf, G. R., Randerson, J. T., Giglio, L., Collatz, G. J., Kasibhatla, P. S., and Arellano Jr.,
963 A. F.: Interannual variability in global biomass burning emissions from 1997 to 2004, Atmos.
964 Chem. Phys., 6, 3423–3441, https://doi.org/10.5194/acp-6-3423-2006, 2006.

van der Werf, G. R., Randerson, J. T., Giglio, L., Gobron, N., & Dolman, A. J. (2008). Climate controls on the variability of fires in the tropics and subtropics. Global Biogeochemical Cycles, 22(3).

Walker, X. J., Rogers, B. M., Veraverbeke, S., Johnstone, J. F., Baltzer, J. L., Barrett, K., ... & Goetz, S. (2020). Fuel availability not fire weather controls boreal wildfire severity and carbon emissions. Nature Climate Change, 1-7.

Wang, X., Studens, K., Parisien, M. A., Taylor, S. W., Candau, J. N., Boulanger, Y., & Flannigan, M. D. (2020). Projected changes in fire size from daily spread potential in Canada over the 21st century. Environmental Research Letters, 15(10), 104048.

Ward, D. S., Kloster, S., Mahowald, N. M., Rogers, B. M., Randerson, J. T., and Hess, P. G.: The changing radiative forcing of fires: global model estimates for past, present and future, Atmos. Chem. Phys., 12, 10857–10886, https://doi.org/10.5194/acp-12-10857-2012, 2012.

Wiedinmyer, C., Quayle, B., Geron, C., Belote, A., McKenzie, D., Zhang, X., O'Neill, S., and Wynne, K. K.: Estimating emissions from fires in North America for air quality modeling, Atmos. Environ., 40, 3419–3432, doi:10.1016/j.atmosenv.2006.02.010, 2006.

Xia, L., Robock, A., Tilmes, S., and Neely III, R. R.: Stratospheric sulfate geoengineering could enhance the terrestrial photosynthesis rate, Atmos. Chem. Phys., 16, 1479–1489, https://doi.org/10.5194/acp-16-1479-2016, 2016.

Xia, L., Nowack, P. J., Tilmes, S., and Robock, A.: Impacts of stratospheric sulfate geoengineering on tropospheric ozone, Atmos. Chem. Phys., 17, 11913–11928, https://doi.org/10.5194/acp-17-11913-2017, 2017.

Xu, Y., Lin, L., Tilmes, S., Dagon, K., Xia, L., Diao, C., Cheng, W., Wang, Z., Simpson, I., and Burnell, L.: Climate engineering to mitigate the projected 21st-century terrestrial drying of the Americas: a direct comparison of carbon capture and sulfur injection, Earth Syst. Dynam., 11, 673–695, https://doi.org/10.5194/esd-11-673-2020, 2020.

Yue, C., Hantson, S., Ciais, P., & Laurent, P. (2016). Evaluating FireMIP models over boreal regions. *in the FireMIP 2016 Workshop*.

Zhang, L., W. Lau, W. Tao, and Z. Li. "Large Wildfires in the Western United States Exacerbated by Tropospheric Drying Linked to a Multi - Decadal Trend in the Expansion of the Hadley Circulation." Geophysical Research Letters 47, no. 16 (2020): e2020GL087911.

Zhang, Y., Fan, J., Shrivastava, M., Homeyer, C.R., Wang, Y. and Seinfeld, J.H., 2022. Notable impact of wildfires in the western United States on weather hazards in the central United States. Proceedings of the National Academy of Sciences, 119(44), p.e2207329119.

Deleted:

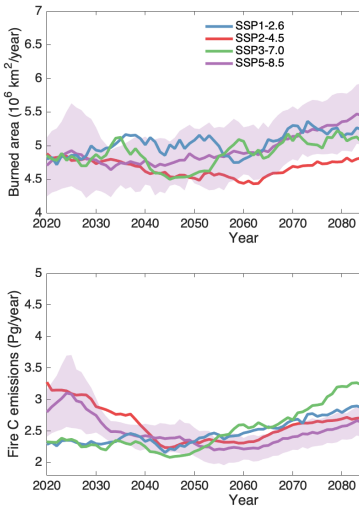

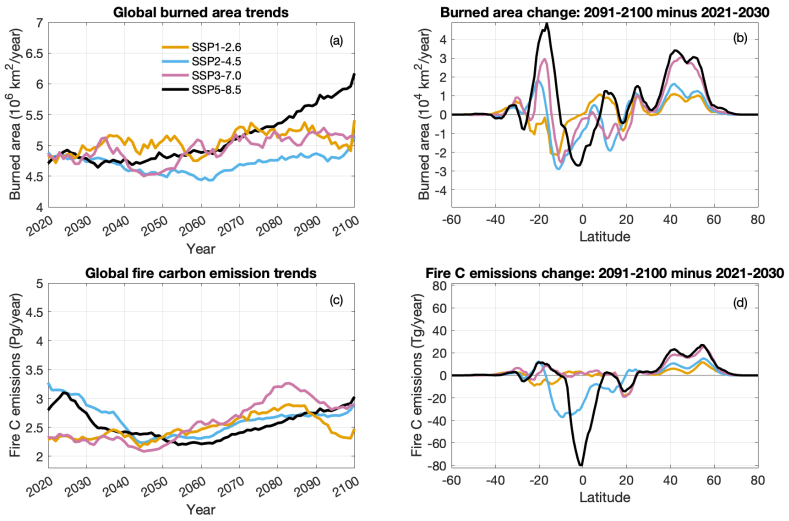

Figure 1. Overall global burned area and fire carbon emission trends and changes under SSP scenarios. (a) Time series of global burned area from 2020 to 2100 under the SSP1-2.6, SSP2-4.5, SSP3-7.0, and SSP5-8.5 scenarios (represented by different colors). The time series are shown as 5-year moving averages. (b) Zonal changes (absolute value) of burned area in the period 2091-2100 relative to the period 2021-2030 (calculated by the value in 2091-2100 minus the value in 2021-2030), under the SSP1-2.6, SSP2-4.5, SSP3-7.0, and SSP5-8.5 scenarios (represented by different colors, color code is the same as it in panel a). 5-degree moving average were applied to the shown zonal changes. Panels (c) and (d) are similar to panels (a) and (b), respectively, but for fire carbon emissions.

Deleted: For the scenarios with multiple simulations, the ranges are also shown by the shaded areas.

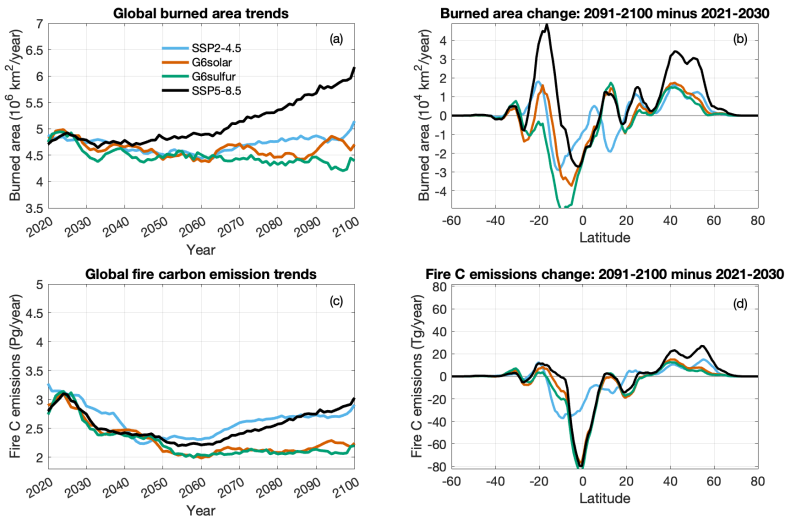

Figure 2. Overall global burned area and fire carbon emission trends and changes under the G6sulfur and G6solar geoengineering scenarios relative to SSP2-4.5 and SSP5-8.5. (a) Time series of global burned area from 2020 to 2100 under the G6sulfur, G6solar, SSP2-4.5, and SSP5-8.5 scenarios (represented by different colors). The time series are shown as 5-year moving averages. (b) Zonal changes (absolute value) of burned area in the period 2091-2100 relative to the period 2021-2030 (calculated by the value in 2091-2100 minus the value in 2021-2030), under the G6sulfur, G6solar, SSP2-4.5, and SSP5-8.5 scenarios (represented by different colors, color code is the same as it in panel a). 5-degree moving average were applied to the shown zonal changes. Panels (c) and (d) are similar to panels (a) and (b), respectively, but for fire carbon emissions.

Deleted:

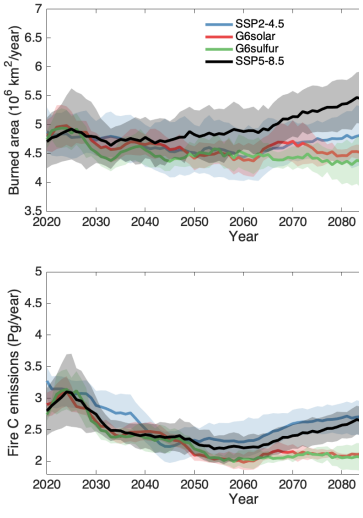

Deleted: For the scenarios with multiple simulations, the ranges are also shown by the shaded areas.

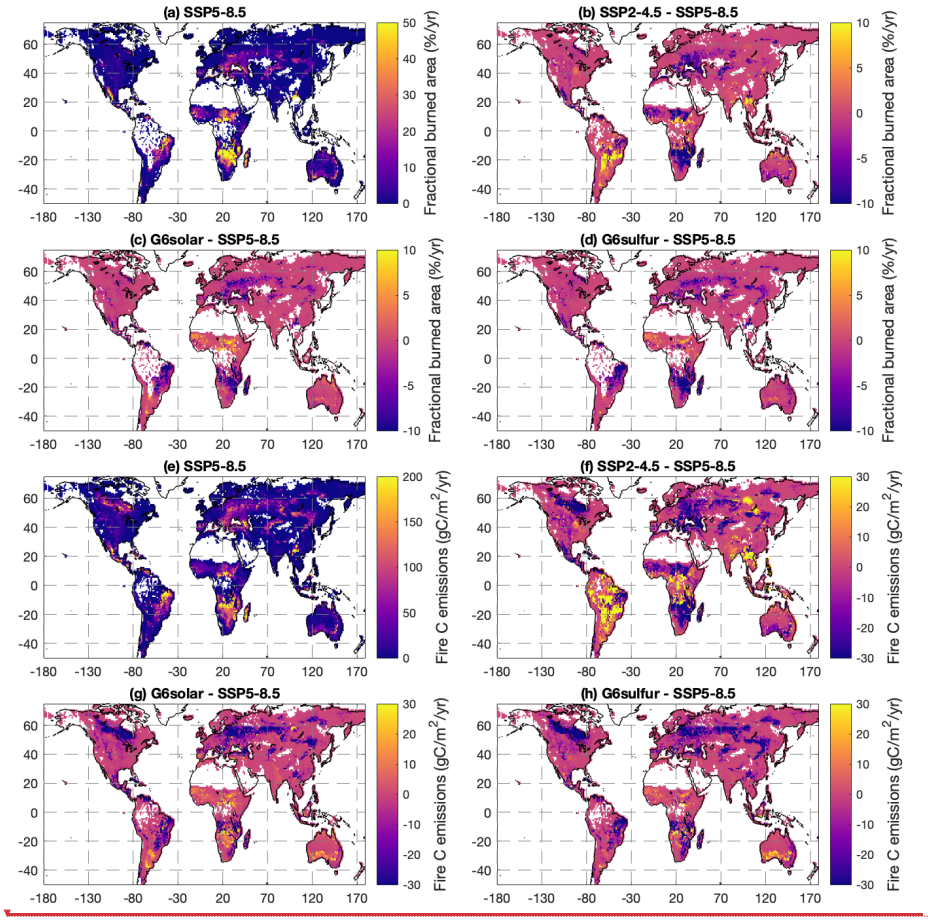

Figure 3. Fractional burned area (%/year) and fire carbon missions (gC/m^2/year) averaged for 2091-2100. (a) Spatial distribution of fractional burned area (%/year) averaged for 2091-2100 under SSP5-8.5. Results are not shown for model grids where fractional burned area equals to 0. The difference in fractional burned area of (b) SSP2-4.5 from SSP5-8.5 (c) G6Solar from SSP5-8.5, and (d) G6Sulfur from SSP5-8.5 averaged for 2091-2100. Results are not shown for model grids where the difference in fractional burned area equals to 0. (e-h) are similar to (a-d) but for fire carbon missions (gC/m^2/year). For a scenario with multiple simulations (i.e., SSP5-8.5, SSP2-4.5, G6Sulfur, and G6Solar), simulation mean is shown.

Deleted:

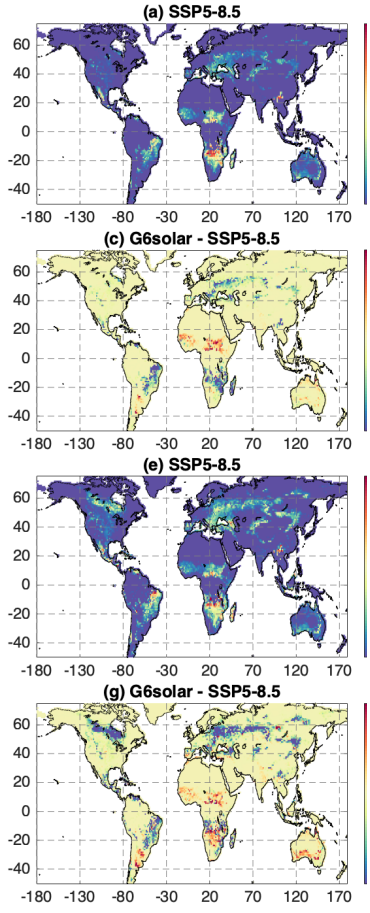

Deleted: surface temperature

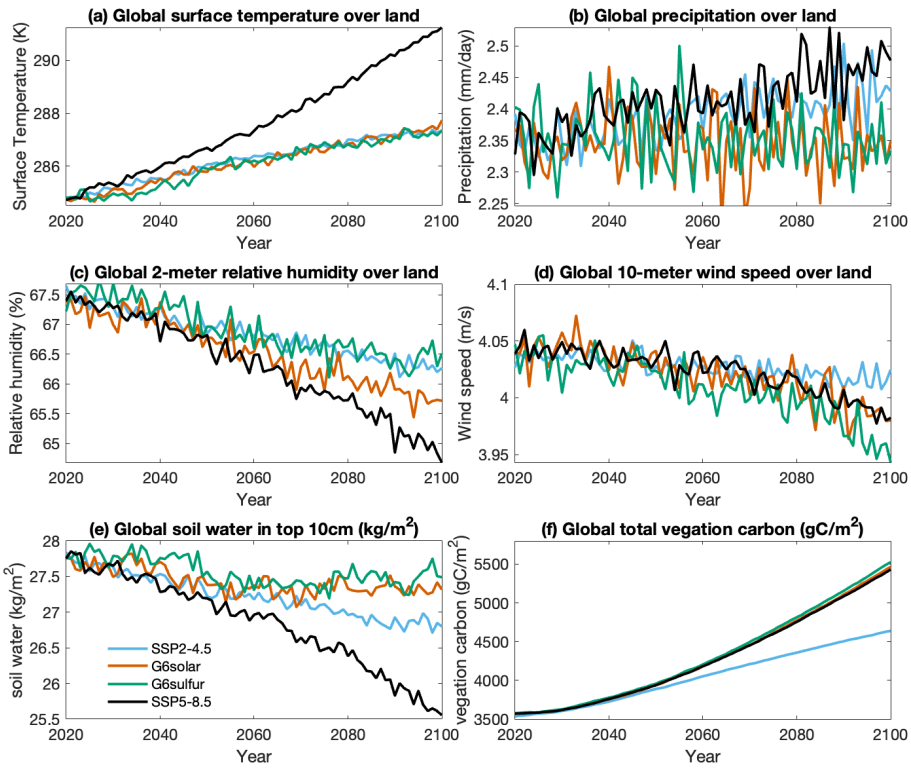

Figure 4. Time series of mean (a) surface temperature (K), (b) precipitation (mm/day) over the land, (c) 2-meter relative humidity (%) over the land, (d) 10-meter wind speed (m/s) over the land, (e) soil water content at top 10 cm (kg/m^2), and (f) vegetation carbon excluding carbon pool (Gc/m^2). For a scenario with multiple simulations (i.e., SSP5-8.5, SSP2-4.5, G6Sulfur, and G6Solar), simulation means are shown.

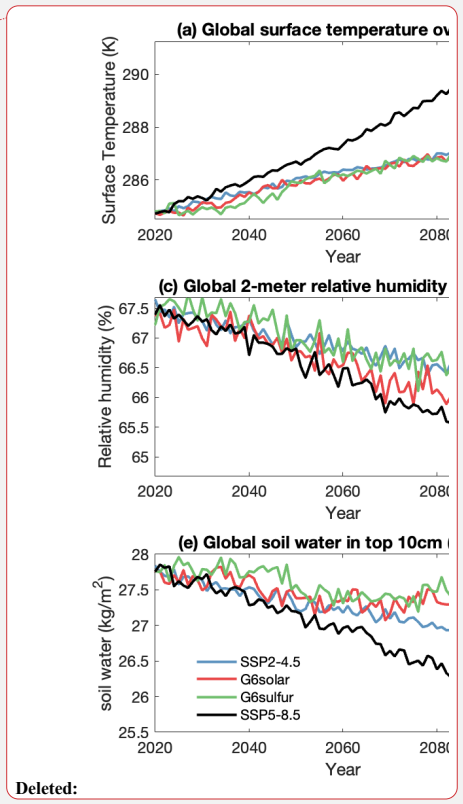

Deleted:

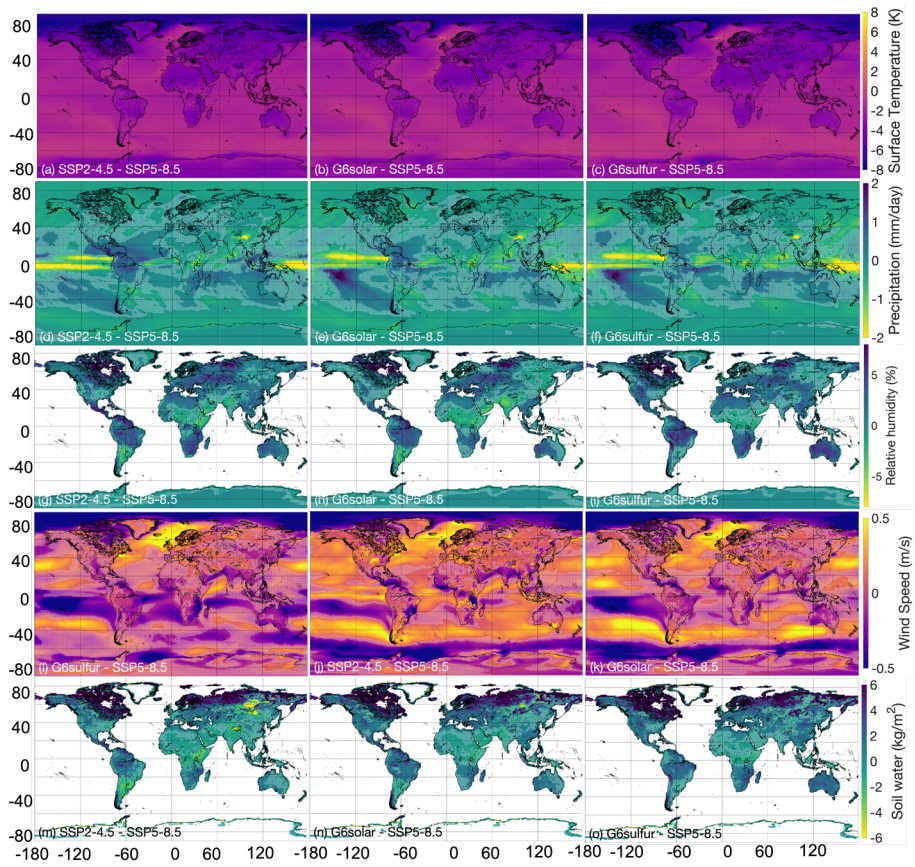

Figure 5. The difference in surface temperature (K) of (a) SSP2-4.5 from SSP5-8.5 (b) G6Solar from SSP5-8.5, (c) G6Sulfur from SSP5-8.5 averaged for 2091-2100. (d-f) are the same as (a-c) but for precipitation (mm/day). (g-i) are the same as (a-c) but for 2-meter relative humidity (%). (j-l) are the same as (a-c) but for 10-meter wind speed (m/s). (m-o) are the same as (a-c) but for soil water content at top 10 cm (kg/m^2). The grids where SSP2-4.5, G6Sulfur, or G6Solar is not significantly different from SSP5-8.5 is marked with white shade. Taking precipitation of SSP2-4.5 as an example, the significance for each model grid is calculated by student t-test (p value is 0.1) using 10 years of SSP2-4.5 precipitation data during 2091-2100 (10 data points) and 10 years of SSP5-8.5 precipitation data during 2091-2100 (10 data points).

Deleted:

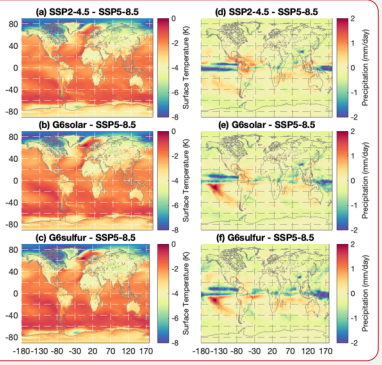

Deleted: ¶
¶

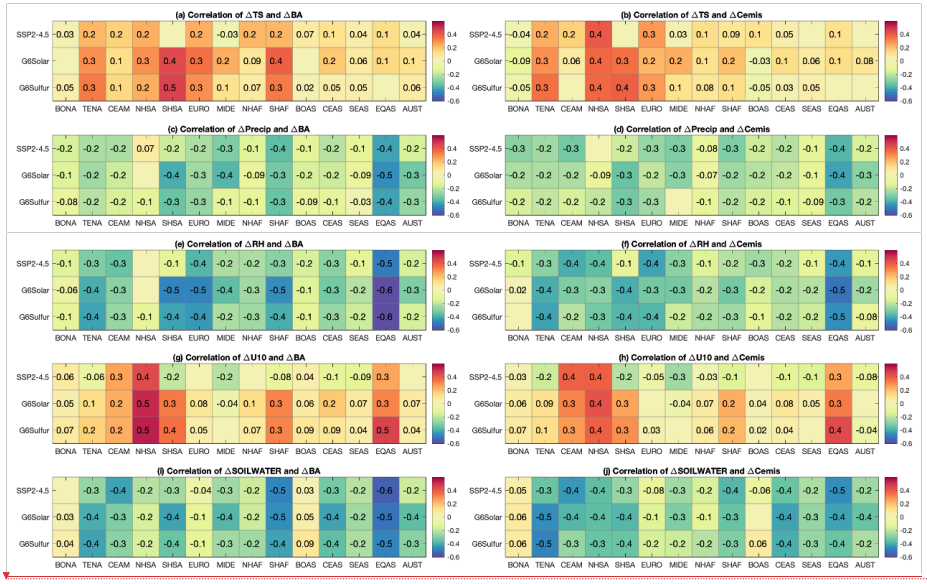

Figure 6. Correlations of (a) surface temperature change (ΔTS) and burned area change for SSP2-4.5, G6Solar, and G6Sulfur, and (b) ΔTS and fire carbon emission change (ΔCemis) for SSP2-4.5, G6Solar, and G6Sulfur. Only correlations that are significant are labeled (p value <= 0.1). For SSP2-4.5, ΔTS is calculated for individual model grids within the region and annual values. It is defined as TS of SSP2-4.5 minus TS of SSP5-8.5 (the reference case). For G6Solar and G6Sulfur, ΔTS is defined in the same way as SSP2-4.5. ΔBA and ΔCemis are defined in the same way as ΔTS. (c-d) are the same as (a-b) but for precipitation change (ΔPrecip). (e-f) are the same as (a-b) but for relative humidity change (ΔRH). (g-h) are the same as (a-b) but for 10-meter wind speed change (ΔU10). (i-j) are the same as (a-b) but for the change in soil water content at top 10 cm (ΔSOILWATER). Correlations are calculated for 14 fire regions (x-axis), following Giglio et al. (2010), namely Boreal North America (BONA), Temperate North America (TENA), Central America (CEAM), Northern Hemisphere South America (NHSA), Southern Hemisphere South America (SHSA), Europe (EURO), Middle East (MIDE), Northern Hemisphere Africa (NHAF), Southern Hemisphere Africa (SHAF), Boreal Asia (BOAS), Central Asia (CEAS), Southeast Asia (SEAS), Equatorial Asia (EQAS), and Australia and New Zealand (AUST). The definition of the regions can be found in Figure S3.

Deleted:

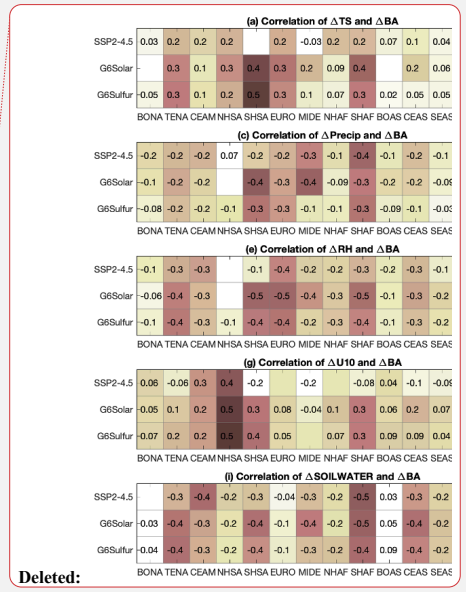

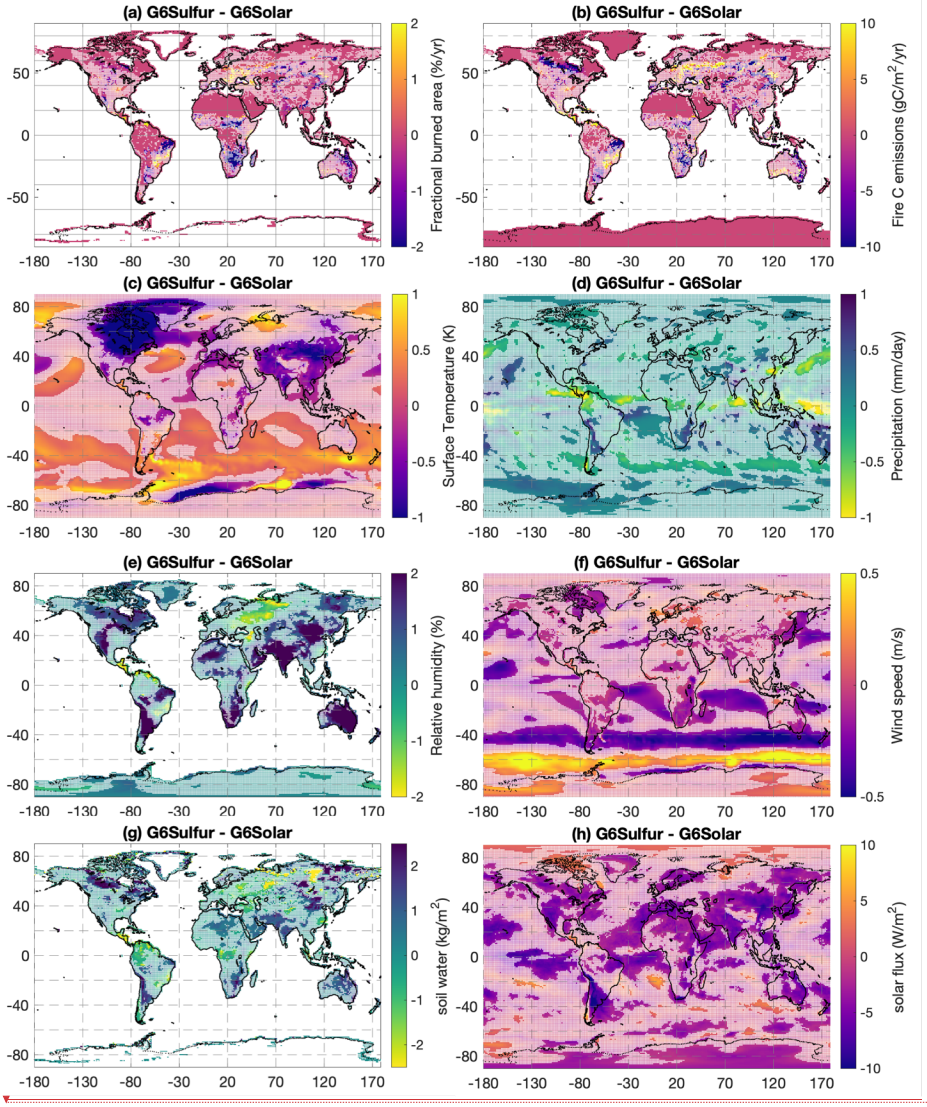

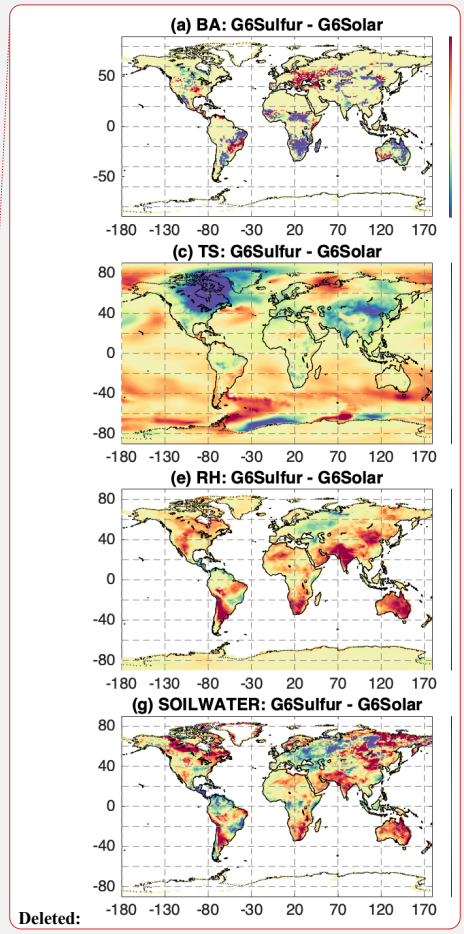

Deleted:

Figure 7. The difference between G6Sulfur and G6Solar in (a) burned area fraction (BA; %/yr), (b) fire carbon emissions (Cemis; gC/m^2/yr), (c) surface temperature (TS; K), (d) precipitation (Precip; mm/day), (e) 2-meter relative humidity (RH; %), (f) 10-meter wind speed (U10; m/s), (g) soil water content at top 10 cm (Soilwater; kg/m^2), and (h) downwelling solar flux at the surface (FSDS; W/m^2) averaged for 2091-2100. The grids where SSP2-4.5, G6Sulfur, or G6Solar is not

significantly different from SSP5-8.5 is marked with white shade. Taking precipitation of SSP2-4.5 as an example, the significance for each model grid is calculated by student t-test (p value is 0.1) using 10 years of SSP2-4.5 precipitation data during 2091-2100 (10 data points) and 10 years of SSP5-8.5 precipitation data during 2091-2100 (10 data points).

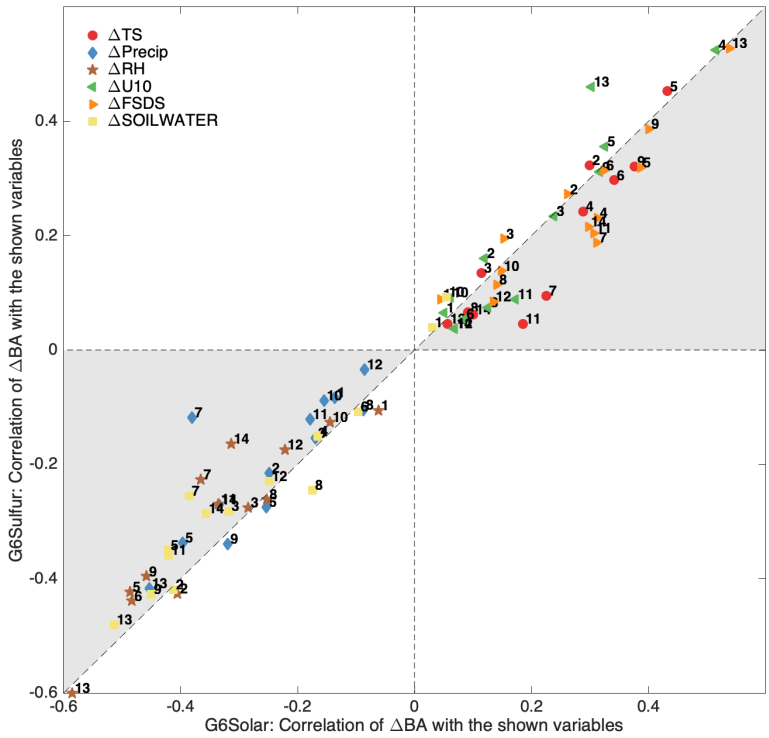

Figure 8. Correlations between burned area change in G6Solar from SSP5-8.5 (ΔBA) with the change in other variables in G6Solar from SSP5-8.5 (x-axis) versus correlations between burned area change in G6Sulfur from SSP5-8.5 (ΔBA) with the change in other variables in G6Sulfur from SSP5-8.5 (y-axis). The variables shown here are surface temperature change (ΔTS), precipitation change (ΔPrecip), 2-meter relative humidity change (ΔRH), 10-meter wind speed change (ΔU10), soil water content in top 10 cm change (ΔSOILWATER), and downwelling solar flux at the surface change (ΔFSDS). All "changes" refer to 2091-2100 averages. The numbers labeled in the figure correspond to the region: 1–Boreal North America, 2–Temperate North America, 3–Central America, 4–Northern Hemisphere South America, 5–Southern Hemisphere South America, 6–Europe, 7–Middle East, 8–Northern Hemisphere Africa, 9–Southern Hemisphere Africa, 10–Boreal Asia, 11–Central Asia, 12–Southeast Asia, 13–Equatorial Asia, and 14–Australia and New Zealand. The definition of the regions can be found in Figure S3. The shade highlights where correlation with ΔBA is larger than correlation with ΔCemis. See Figure S13 for plots with variables separately presented.

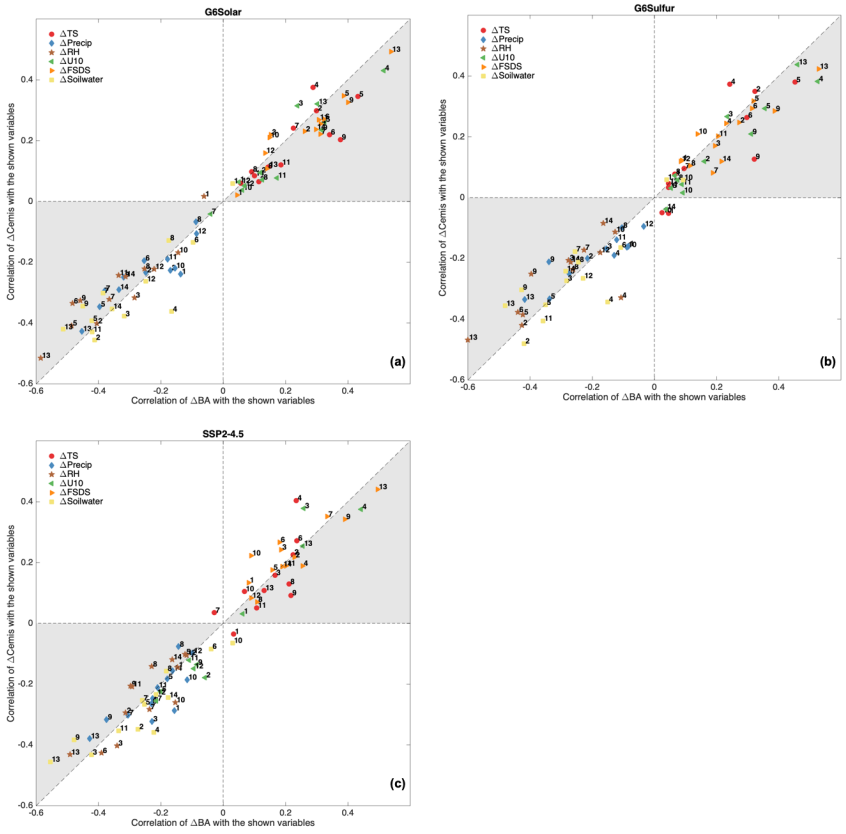

Deleted: G6Solar

Figure 9. (a) Correlations between burned area change in G6Solar from SSP5-8.5 (ΔBA) with the change in other variables in G6Solar from SSP5-8.5 (x-axis) versus correlations between fire carbon emission change in G6Solar from SSP5-8.5 (ΔCemis) with the change in other variables in G6Solar from SSP5-8.5 (y-axis). The variables shown here are surface temperature change (ΔTS), precipitation change (ΔPrecip), 2-meter relative humidity change (ΔRH), 10-meter wind speed change (ΔU10), soil water content in top 10 cm change (ΔSOILWATER), and downwelling solar flux at the surface change (ΔFSDS). All "changes" refer to 2091-2100 averages. The numbers labeled in the figure correspond to the region: 1–Boreal North America, 2–Temperate North America, 3–Central America, 4–Northern Hemisphere South America, 5–Southern Hemisphere South America, 6–Europe, 7–Middle East, 8–Northern Hemisphere Africa, 9–Southern Hemisphere Africa, 10–Boreal Asia, 11–Central Asia, 12–Southeast Asia, 13–Equatorial Asia, and 14–Australia and New Zealand. The definition of the regions can be found in Figure S3. The shade highlights where correlation with ΔBA is larger than correlation with ΔCemis. (b) is the same as (a) but for G6Sulfur. (c) is the same as (a) but for SSP2-4.5. See Figure S14-S16 for plots with variables separately presented.

Deleted: BA